2011

Adaptive Sliding Mode Control for Aircraft Engines

Kathryn C. Ebel
Cleveland State University

ADAPTIVE SLIDING MODE

CONTROL FOR AIRCRAFT ENGINES

KATHRYN C EBEL

Bachelor of Science in Mechanical Engineering

Ohio University, Athens, Ohio

August, 2001

submitted in partial fulfillment of requirements for the degree

MASTER OF SCIENCE IN MECHANICAL ENGINEERING

at the

CLEVELAND STATE UNIVERSITY

December, 2011

This thesis has been approved

for the department of MECHANICAL ENGINEERING

and the College of Graduate Studies by:

_____

Thesis Chairperson, Hanz Richter, Ph.D.

_____

Department & Date

_____

Jerzy T Sawicki, Ph.D.

_____

Department & Date

_____

Daniel Simon, Ph.D.

_____

Department & Date

ACKNOWLEDGMENTS

I would like to thank Dr. Hanz Richter for his guidance throughout the duration of this project. As my advisor, Dr. Richter shared his ideas and expertise, which greatly supported the completion of this thesis. I would like to express my appreciation to Dr. Jerzy Sawicki and Dr. Dan Simon for serving on my thesis committee. I would also like to thank the NASA GSRP program for funding this work.

I would like to thank my friends and family for their support. To my family, the support and encouragement you have given me is truly the number one factor in the completion of this thesis.

ADAPTIVE SLIDING MODE CONTROL FOR AIRCRAFT ENGINES

KATHRYN C EBEL

ABSTRACT

Aircraft engine control has been evolving since its beginning. With advancements in technology more and more control methods are being applied to this area. This thesis presents the design of an adaptive PID sliding mode control (A-SMC) for a turbofan engine. The controller design methodology is presented. Using an aircraft engine simulation environment developed by NASA, called Commercial Modular Aero-Propulsion System Simulation, the developed controller is tested. The results from three simulations are analyzed to investigate the application of this new design scheme. The A-SMC is able to follow the demanded fan speed for short flight simulations. However, some of the adaptive gains continue to increase when operating away from the limits. It is shown that using an A-SMC is a feasible methodology for controlling an aircraft engine, although further studies are necessary to investigate the adaptive PID control and the technique chosen to eliminate the chattering phenomenon of sliding mode control.

TABLE OF CONTENTS

LIST OF FIGURES

CHAPTER I

INTRODUCTION

The task of designing control systems for aircraft engines is complex, due to the fact that the systems are inherently nonlinear. However, with advancements in technology, aircraft engines and controller hardware are ever evolving. Along with these improvements new control design methodologies are being investigated. This thesis seeks to study the application of an adaptive PID sliding mode control (A-SMC) to an aircraft engine system. SMC was chosen for its robustness in dealing with variations in system parameters. In addition, an adaptive PID gains technique is applied to help deal with these variations. This first chapter will cover three basic types of aircraft engines and how they work. The controls problem will be introduced along with the challenges faced when designing a control scheme. An overview of the organization of the thesis is also included.

1.1 Aircraft Engines

The turbojet engine was introduced in the 1940s, making it the first jet engine used for aircraft propulsion [6]. It is also the simplest of the three basic types of jet engines. It is comprised of a compressor, a combustor, a turbine to drive the compressor, and an exhaust nozzle. They are capable of obtaining high specific thrust and are best

utilized in high subsonic and supersonic flight speeds [10]. Turbojets can be classified as single or double spool and may have either centrifugal or axial compressors. Also, turbojets can have afterburners, but not all do.

The turboprop engine is similar to the turbojet except that is has an external propeller that is driven by the gas turbine. The total engine airflow is increased with the addition of the propeller. The specific thrust is decreased but the propulsion efficiency is increased. The power of the rotating shaft is optimized and not the thrust produced by the exhaust. The propeller's speed is controlled by a gearbox that is connected to the shaft. Turboprop engines can be classified into two groups. In the first group, the gas turbine that drives the compressor is also used to drive the propeller. An additional free power turbine can also be used to drive the propeller. Turboprop engines are mostly used in helicopters and small, low speed aircrafts [10]. The engine used in helicopters is sometimes referred to as a turboshaft engine. The distinction between the two is based on the location of the gearbox. For a turboshaft engine it is part of the vehicle, while in a turboprop it is part of the engine itself.

The turbofan engine is a compromise between turbojets and turboprops [6]. The turbofan has a compressor, a combustor, and a turbine. It also has a fan and a second turbine to drive the fan. A portion of the airflow from the intake is passed through the core of the engine, as it is in the previous engines. A second stream of air is bypassed around the core. This stream is substantially larger than that passed through the core. This approach also reduces the specific thrust and increases the propulsion efficiency, which reduces fuel consumption. These advantages are why turbofans are widely used for large commercial aircrafts. There are a few different classifications for turbofan engines. A turbofan can have one, two, or three spools. The fan can be either a forward fan or an aft fan. The bypass ratio (BPR) may be high or low. A low BPR engine is further divided into afterburning or nonafterburning. Also, the air that is bypassed is either exhausted through a separate nozzle or it is mixed back

with the hot stream and both are exhausted through the same nozzle [18]. This is referred to as unmixed or mixed. Unmixed types are further divided into having short or long ducts.

All types of jet engines operate on a Brayton cycle. This is a continuous flow process that ideally has isentropic compression and constant pressure combustion. The processes of the turbofan engine will serve as an overview of how an aircraft engine works.

Air is taken in through the inlet where the air is compressed. This air passes through the fan where it is then separated into two streams of air. One stream is bypassed around the core and is exhausted through a separate nozzle (unmixed). The other stream, sometimes referred to as the "hot stream," is supplied to the compression system. Next the fuel is burned in the combustor and passed along to the turbines. The gas expands in the turbines which produces power for the compression system. The high pressure turbine drives the compressor while the low pressure turbine drives the fan. The stream then flows to the nozzle where it expands further to ambient air pressure. This is what provides the thrust for the engine.

1.2   Controls Problem

The main objective of the control system for an aircraft engine is to produce the desired thrust based on the position of the throttle. The simplest way to do this is by controlling the fuel flow. Since in flight calculation of thrust is not currently practical, other means of management are required. Shaft rotational speed (N_f) and engine pressure ratio (epr) have each been proven as good indicators of an engine's thrust [18].

The controller is required to attain the desired thrust while operating within the limits of the engine. The limits of the engine include: (1) maximum fan speed,

(2) maximum compressor speed, (3) maximum turbine temperature, (4) fan stall, (5) compressor stall, (6) maximum compressor discharge pressure, and (7) minimum compressor discharge pressure. In order for the engine to operate at maximum power, the engine will have to operate at one or more of these limits. Therefore, the controller must be able to evaluate these parameters and possibly limit the thrust so that none of them are exceeded.

Aircraft engines operate in a wide range of conditions. These ranges include altitude from sea level to 50,000 feet and Mach numbers from static to high subsonic speed [18]. Also, the ambient temperature can vary causing an even wider range of variations to the flight envelope. The engine models are greatly effected by this and are constantly changing throughout the course of an aircraft's flight.

1.3   Scope of Thesis

The purpose of this thesis is to investigate the applicability of an adaptive PID sliding mode control (A-SMC) to an aircraft engine. The controller scheme developed here will be tested in a simulation environment developed by NASA. The Commercial Modular Aero-Propulsion System Simulation (C-MAPSS) [8] represents a generic, high bypass, two-spool turbofan engine. After the controller is implemented, different operating conditions will be simulated to test the robustness of the controller.

The remainder of this thesis is broken down into five chapters. Chapter 2 will cover engine models and simulation. This will include what is involved in building a model of an engine. A look at simulation tools, including an in depth look at C-MAPSS, will be presented. The concept of sliding mode control will be presented in Chapter 3. An example of an SMC controller will be given. The undesirable phenomenon of chattering that is present in SMC systems will be discussed. Chapter 4 will cover the basic concepts of adaptive control and will build on the concepts of Chapter 3

by including the adaptive gain portion of the A-SMC control law. The developed controller will then be implemented in C-MAPSS and presented in Chapter 5. The results of different simulations will be discussed. Chapter 6 will summarize the results of this study and provide recommendations for future work.

CHAPTER II

AIRCRAFT ENGINES

2.1 Introduction

This chapter gives a brief overview of the components of an aircraft engine, engine controls, and some simulation tools that are available. The function and characteristics of each component are presented along with the processes of the ideal Brayton cycle. Core speed control was the first method used for designing aircraft engine controls. However, this proved to be less than ideal. Now, thrust management is controlled using fan speed or engine pressure ratio.

2.2 Aircraft Engine Components

A diagram of an aircraft engine is shown in Figure 2.1. The cold section contains the inlet and compressors. The combustor, turbines, and nozzle are referred to as the hot section. The main components are highlighted and an overview of the Brayton Cycle is presented.

INTAKE   COMPRESSION   COMBUSTION   EXHAUST

Air Inlet   Combustion Chambers   Turbine

Cold Section   Hot Section
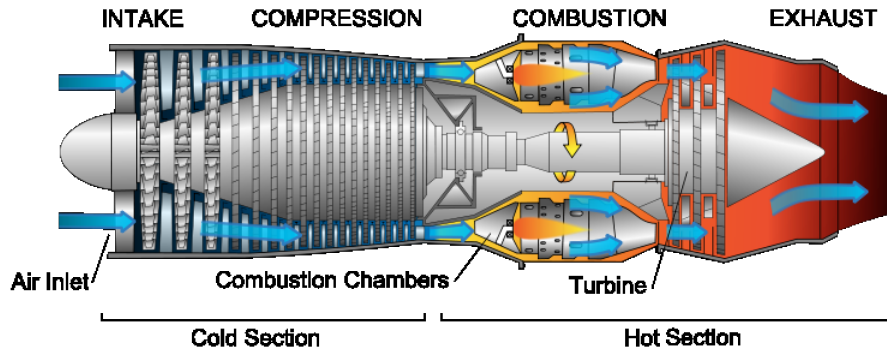
Figure 2.1: Diagram of an Aircraft Engine (from [7])

2.2.1 Inlet

The inlet of an aircraft engine supplies atmospheric air to the engine. Efficient propulsion of the engine relies on the inlets ability to capture the air with as little distortion as possible. Also, the inlet must be designed so that the external flow around the engine causes minimal external drag. The inlet is designed by the manufacturers of the airframe and not by the engine manufacturers. However, both are involved in the testing of the inlet because the compatibility of the inlet and the engine is essential. Different inlets are used for subsonic and supersonic engines.

Subsonic inlets have a smooth continuous surface that is relatively thick at the lip. The most common type is the pitot inlet. It is made up of a forward entry hole with a cowl lip. There are three major types of pitot inlets. Transport aircrafts use podded inlets. Integrated inlets can be found on combat aircraft. And, flush inlets are used on missiles because they can easily be integrated into the missile's airframe.

Supersonic inlets have a supersonic diffuser and a subsonic diffuser. The supersonic diffuser decelerates the flow with a combination of shocks and diffuse compression. The subsonic diffuser is able to reduce the Mach number to a level that is acceptable by the engine. Supersonic inlets can be classified in a couple of ways. Axisymmetric inlets use a cone shape to shock the flow down to subsonic speeds, whereas

7

the two-dimensional type has a rectangular cross-section. Fixed-geometry inlets have a constant cross-sectional area. Variable geometry types are able to adjust the size of the cross-sectional area by either moving the cone fore-and-aft (axisymmetric) or through the use of hinged flaps (two-dimensional). Internal, external, or mixed compression types refer to the location of the shocks: between the nose lip and inlet throat (internal), between the forebody and the inlet lip (external), or in both locations (mixed).

2.2.2   Compressor

Centrifugal compressors are used in small aircraft engines. The three main parts of the compressor are the impeller, diffuser, and manifold. The impeller draws in air at its center and accelerates it with fast spinning speed. The air is then thrown out at its tip. These passages on the impeller diffuse the flow to a lower relative velocity and a high static pressure. The air is discharged by the diffuser with a high absolute velocity. The goal is to reduce the kinetic energy which increases the static pressure. All diffusers have a vaneless passage, however, some are followed by a vaned section. The vaned section can be either cascade, channel or pipe types. The final element of the compressor is the manifold. The diffuser is often bolted to the manifold in applications where the compressor is followed by a combustion chamber, as in aircraft engines.

Centrifugal compressors may be single or multiple stage. Single entry and dual entry differ in the size of the impeller and the ducting arrangement. Single entry allows ducting directly to the inducer vanes. Dual entry involves more complicated ducting to reach the rear side. Due to its smaller size and higher rotational speeds, the dual entry is the type found on most aircrafts today. The impeller may be shrouded or unshrouded. A shrouded impeller has a rotating shroud that is fixed to the vanes. An unshrouded impeller has a clearance between the tips and a stationary shroud;

this is the type that is typically used.

Axial-flow compressors are used in all types of aircraft engines. The air flows along the axis of rotation. Axial compressors have large mass flow capacity, high reliability, and high efficiency. The pressure rise per stage is smaller, however, this can be increased by linking stages together. Axial compressors consist of multiple stages of rotor blades on a disc followed by a ring of stator blades. These stages are placed in a row along the power shaft. The purpose of the stator blades is to keep the air from rotating with the rotor blades. The air is accelerated by the rotor blades and then diffused by the stator blades, thus compressing the air. The main parts of an axial compressor are the front frame, casing, rotor assembly, and rear frame.

2.2.3   Combustor

Heat is added to the air in the combustor, sometimes called the burner. The heat is supplied by a direct-fired air heater where the fuel is burned. This is a continuous process that takes place at high pressure in a small space. An electric spark is required for ignition but the flame must be self-sustaining. This can lead to difficulties in the design process on top of the complication of combining the aerodynamics, chemical reaction, and mechanical design of the chamber. The combustion chambers for subsonic and supersonic differ. A combustor can be classified as axial flow, reverse flow, or cyclone types. Axial flow combustors can be further divided into can, can-annular, or annular types. Subsonic combustors have three zones: recirculation zone, burning zone, and dilution zone.

2.2.4   Turbine

Most turbines found in aircraft engines are the axial type. Essentially, the turbine is the same as an axial compressor just operating in reverse. A turbine is composed of a few stages of two successive stators and rows of rotor blades that are air-foil

shaped. Again, the stators keep the air from spiralling around and force the flow parallel to the axis. The majority of the energy extracted from the fluid is turned into mechanical energy which drives the shaft connected to the compressor (or in some cases the fan). As the energy is extracted, the pressure drops. A shroud is placed at the tip of the blade to reduce the leakage of the flow and to reduce blade vibrations. Two key elements in designing a turbine are the high operating temperatures and the high rotating speed. These make the turbine one of the most stressed parts of the engine.

2.2.5 Nozzle

As the air exits the turbine at high velocity it enters the nozzle. In the nozzle the air expands to atmospheric pressure and is exhausted, producing thrust. The primary function is one of transformation of energy and not one of merely transferring the air [11]. Two types of nozzles are convergent and convergent-divergent. An unmixed engine has two separate nozzles, one for the core stream and one for the fan stream. Axisymmetric nozzles direct thrust along the axis of the engine. Two-dimensional nozzles are capable of directing the thrust to adjust the direction of the nose of the plane. Variable geometry nozzles have the ability to reduce the nozzle area which increases the exhaust velocity and thrust. The nozzle can also be fixed geometry. Most subsonic commercial aircrafts use fixed-convergent nozzles which are the simplest form since there are no moving parts.

2.2.6 Brayton Cycle

All types of aircraft engines operate on a Brayton Cycle. A diagram of the ideal Brayton Cycle is shown in Figure 2.2. The steps of the cycle are

- $1 \rightarrow 2$ Isentropic compression: air enters the compressor where temperature
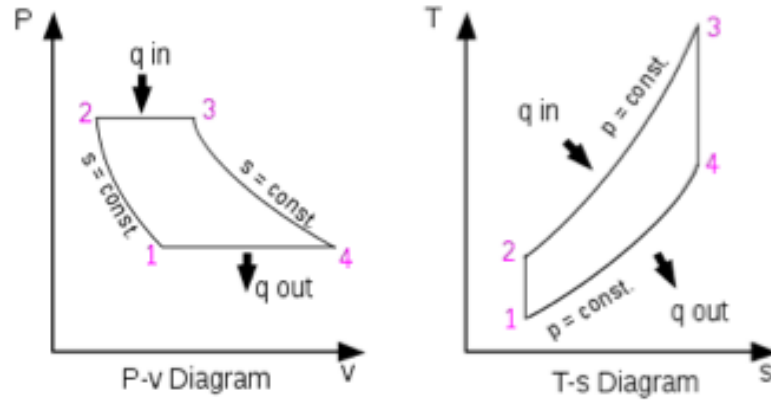
Figure 2.2: Diagram of Brayton Cycle (from [2])

and pressure increase

- $2 \to 3$ Constant heat addition: the fuel is mixed with the high pressure air and burned at constant pressure

- $3 \to 4$ Isentropic expansion: high temperature gas expands in the turbine and drops to atmospheric pressure

- $4 \to 1$ Constant pressure heat rejection: the gas is exhausted to the atmosphere

2.3 Engine Control

2.3.1 Core Speed Control

During the initial stages of aircraft engine control, core speed was used to measure the desired output. There are two different controllers within the core speed control, a steady-state controller and a transient controller [10]. The desired core speed is a function of inlet temperature and throttle position. This is established with a core speed demand schedule, which gives engine thrust as a linear function of the throttle angle. The core speed error is found by comparing the desired core speed to the actual speed. A scheduled gain is then applied to find the ratio of fuel flow to compressor exit

11

Figure 2.3: Core Speed Control Block Diagram (from [10])

pressure (ϕ). This results in a change of fuel flow when the signal for the compressor exit pressure is multiplied. This enables the requirements to be met throughout the flight. A typical core speed control block diagram is shown in Figure 2.3.

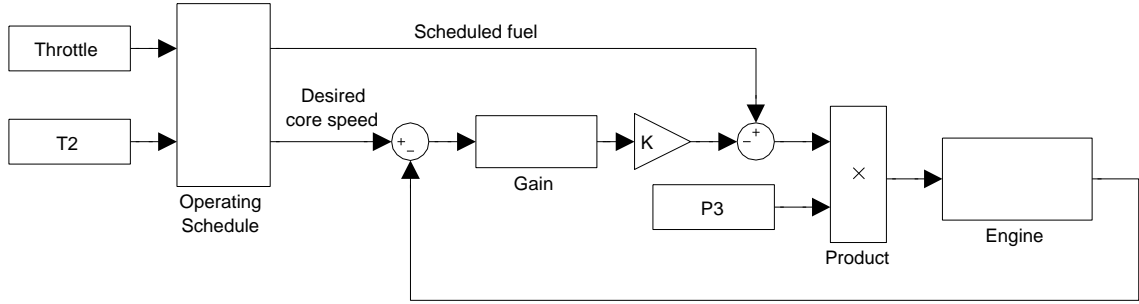The transient controller employs a min-max strategy common in flight control. For engine acceleration, a minimum strategy is used. When the throttle is increased to demand a higher speed a positive error is produced. This results in the fuel valve opening and the engine will accelerate until it reaches the maximum fuel ratio. The min-select will then be governed by the max fuel ratio line until the compressor surge limit is reached. From here, the selection strategy rides the compressor surge limit line at a slower rate of acceleration until it switches back to the maximum fuel ratio line. Acceleration continues on the speed governor line where it reaches the desired steady state operating point.

For a deceleration, a max-select strategy is used. This time there is a negative speed error which closes the fuel valve. The max-select strategy rides the speed governor line until the minimum fuel ratio is met. Once this line meets back with the speed governor line operation will switch back and continue to the steady state operating point.

The use of this min-max strategy allows the engine to operate close to each limit. This results in efficient and rapid control. A complete control block diagram is shown in Figure 2.4.
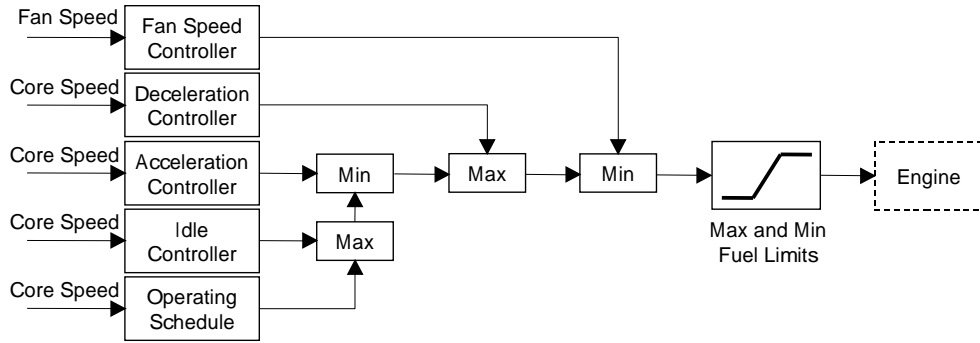
Figure 2.4: Complete Controller Block Diagram (from [10])

2.3.2 Thrust Management

Thrust management requires that thrust be provided as a linear function of throttle position. The controller must be able to obtain the same thrust for a given throttle position regardless of changes to temperature, pressure and Mach at the inlet. More accurate control of aircraft engines can be obtained through control of fan speed or engine pressure ratio. This is due to the fact that thrust is proportional to the airflow through the engine [10]. Only a portion of the airflow travels through the core, whereas all of the air flows through the fan. Likewise, engine pressure ratio, which is the ratio of low pressure turbine pressure to inlet pressure, is also used for control because it directly measures the airflow. As with core speed control, thrust control can be divided into steady-state and transient controls.

2.4 Engine Control Design

2.4.1 Steady-State Control

One of the basic functions of an automatic control system is steady-state control, sometimes called set-point control. The purpose of this part of the controller is to maintain operation at known set points. They are also used to control the engine in
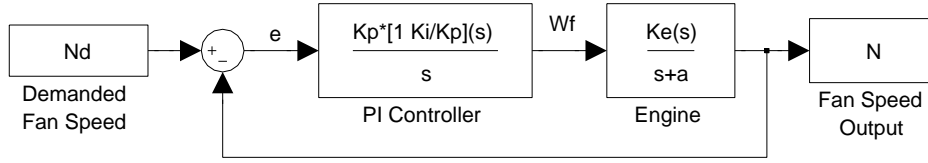
Figure 2.5: Speed Control Loop for a Steady State Controller (from [18])

the area surrounding these set points and to return the control to the center. The steady-state control is designed to operate for long periods of time to hold conditions at the desired point. The following are examples of how a proportional-integral (PI) controller is applied to a one-spool engine from [18].

The simplest gas turbine engine is the one-spool engine. Using fan speed as the power setting variable, the transfer function from fuel flow to fan speed is

$$G(s) = \frac{K_e}{s + a} \tag{2.1}$$

which is a first order lag transfer function. The block diagram for this engine with a PI control law is shown in Figure 2.5. From this, the open loop transfer function can be obtained as

$$OLTF = \frac{K_e K_p (s + K_i/K_p)}{s(s + a)} \tag{2.2}$$

where K_e is the engine gain, K_p is the proportional gain, K_i is the integral gain, and $1/a$ is the time constant of the engine. The first design method applied is the root locus method. This method is a graphical technique for sketching the locus of the roots as a parameter is varied [4]. Stability of the closed loop system is ensured by making sure all of the poles stay on the left hand side of the s-plane. This method is useful because unsatisfactory root locations can easily be identified and changed by varying the parameter.

Following the example from [18], the root locus method is applied to the system in Figure 2.5, where $a = 0.6 \, r/s$ and $K_e = 33 \, rpm/pph$ (where pph is pounds per
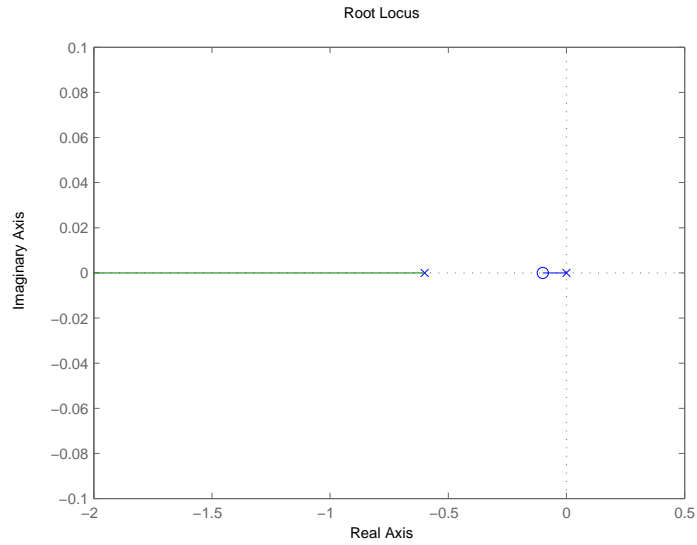
Figure 2.6: Root Locus of One-Spool Engine: Conservative Integrator (from [18])
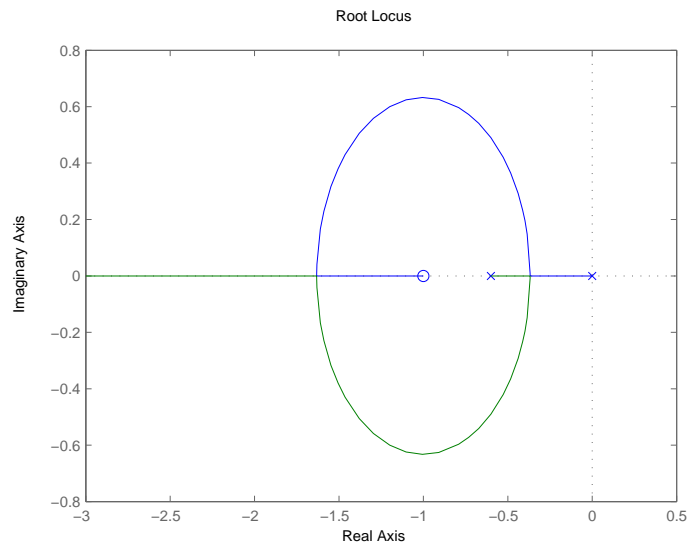
Figure 2.7: Root Locus of One-Spool Engine: Aggressive Integrator (from [18])

hour). Initially the zero is placed at -0.1 for a conservative integrator. The root locus of this system is shown in Figure 2.6. Next, a more aggressive integrator is selected by placing the zero at -1. Figure 2.7 shows the root locus for this system. Here, the closed loop poles are either two real values or two complex conjugates.

Figure 2.8: Step Responses of One-Spool Engine: Small Gain (from [18])

Next, the time responses of the two cases are investigated. The proportional control gain, K_p, is selected to be 0.04 pph/rpm. Figure 2.8 shows the responses of the two cases with a step input applied. It is shown that the response with the aggressive integrator is underdamped. The value of K_p is increased by a factor of 10. Figure 2.9 shows the outputs for a step inp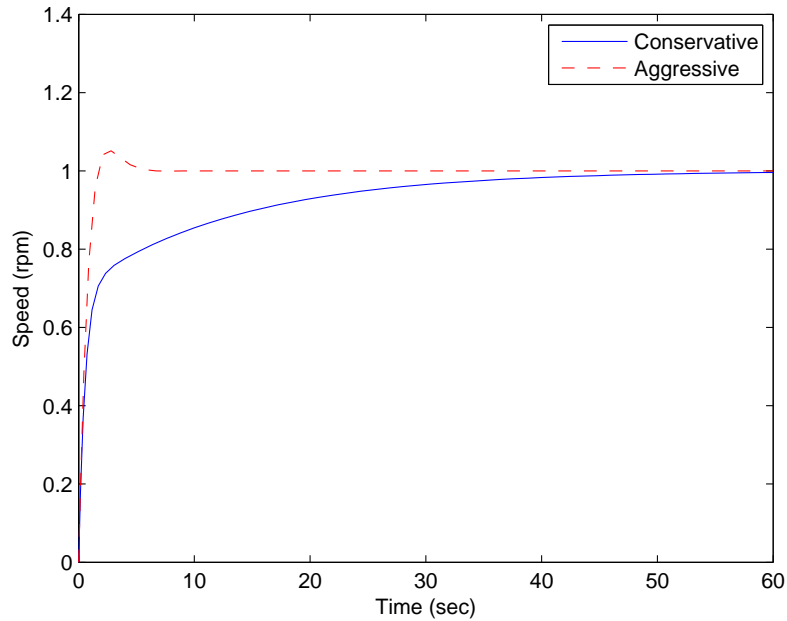ut. Again, the case with the aggressive integrator is underdamped but also has a faster output response. As with any control design, there is a tradeoff among the different objectives. It is up to the designer to decide which characteristics are most desirable.

Another design method that is used in aircraft engine control is the frequency response method. This technique involves shaping the frequency response of the open loop transfer function to meet the desired response characteristics. The first of these characteristics is to have high gains at low frequencies. This allows for disturbance rejection. Also, low gains at high frequencies are desired for noise attenuation and robustness against neglected dynamics. It is desired to have a phase margin greater

16
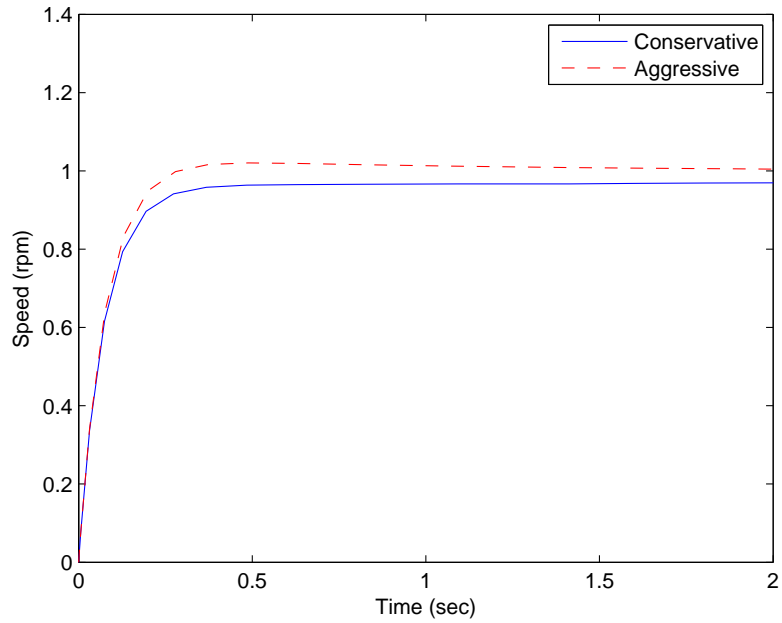
Figure 2.9: Step Responses of One-Spool Engine: High Gain (from [18])

than 45° at the gain crossover frequency. It is also typically desirable to have the slope at the gain crossover frequency be around -20 dB/decade.

To observe the legitimacy of this method, the controller found from the root locus method will be analyzed. The Bode plot for the first case (conservative integrator and $K_p = 0.04$) is shown in Figure 2.10. All of the criteria listed above are met. Also, in Figure 2.11, the Bode plot of the second case (aggressive integrator and $K_p = 0.04$) shows that this case meets the criteria as well.

Figure 2.10: Bode Plot of One-Spool Engine: Conservative Integrator (from [18])

Figure 2.11: Bode Plot of One-Spool Engine: Aggressive Integrator (from [18])

2.4.2 Transient Control and Limit Protection

Another important aspect of automatic control systems is transient control. A gain scheduled controller is used because it can effectively control nonlinear systems. This technique essentially uses the individual steady-state controllers as th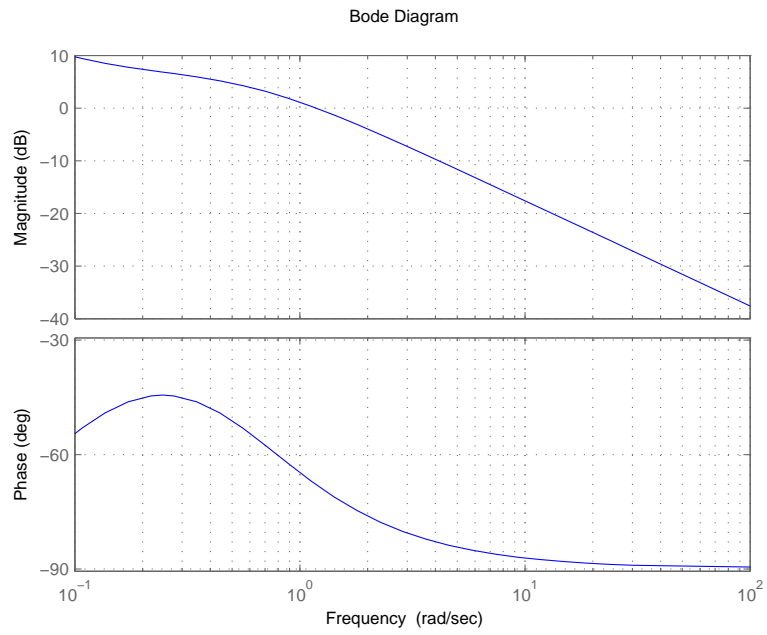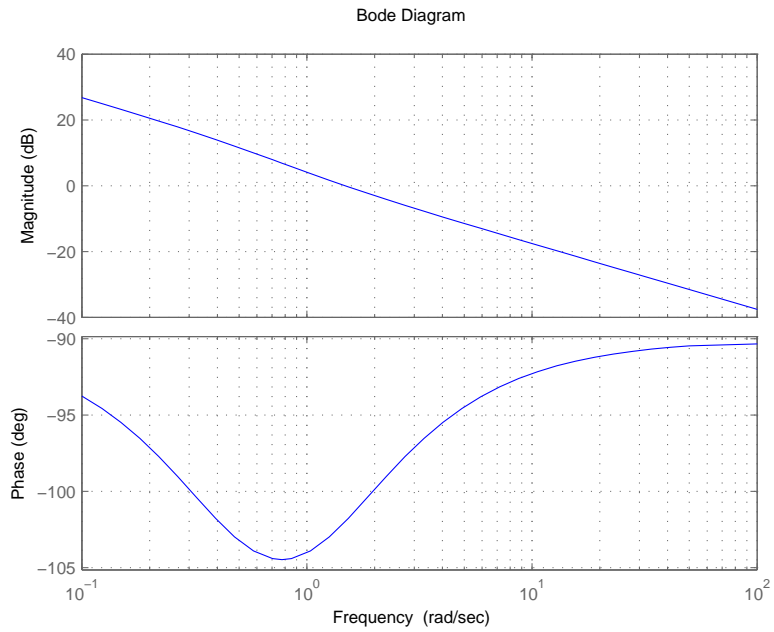e system moves from one operating condition to the next. The structure of the control loop is the same as in steady-state control, however, acceleration and deceleration schedules are added to ensure that the control variable fuel flow does not exceed its limits. A block diagram of the complete transient control logic is shown in Figure 2.12. From the diagram, it is shown that the steady-state control is active as long as it is smaller than the limit in the acceleration schedule, i.e., the smaller of the two is selected. If the change in acceleration is small, this limit may not be reached and only the steady-state controller will be activated. Similarly, for a deceleration of the engine, the steady-state controller is in charge unless it falls below the deceleration limit, in which case the deceleration limit will be larger and will be selected.

The acceleration and deceleration schedules are not the only limitations on an aircraft engine. There are additional limits that protect the engine and its components from undesirable conditions. Unlike the acceleration and deceleration schedules that are active in most large transients, these limit protections are in place only for certain areas of the operating envelope and for unforseen changes in engine performance. To
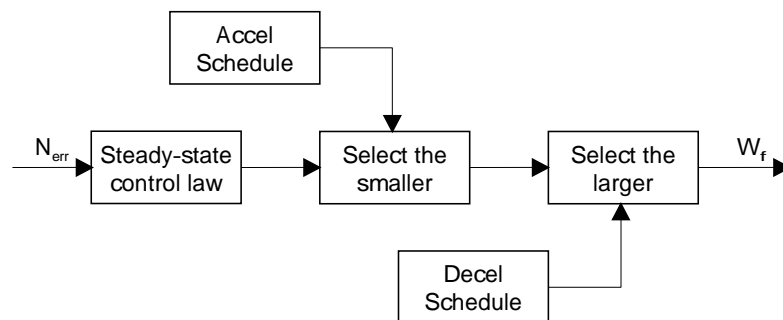

Figure 2.12: Transient Control Logic Block Diagram (from [18])

avoid disk burst or blade break off of the fan shaft, a maximum limit of the physical speed of the shaft must be considered in the controller. Likewise, since the speed of the core shaft is related to that of the fan shaft, a maximum limit must also be placed on the speed of the core shaft. Additionally, a maximum limit is placed on the compressor exit static pressure. Exceeding this limit could result in combustor liner burst. The temperature of the turbines also has a maximum limit. If the temperature in the turbines is allowed to get too high, erosion of the blades can occur. Commonly, these limits are protected by applying a PID controller to each of the output variables. The feedback error used is the difference between the limit value and the engine output. These regulators, along with the controller for thrust management, are placed in a min-max structure.

2.5 Simulation Tools

High fidelity engine simulations have been developed to aid in the research of controls and health management. The National Aeronautics and Space Administration (NASA) has been working on developing non-proprietary simulation tools to provide a common platform to be used across the industry for propulsion system control and diagnostic technology.

The first of these tools to be discussed is the Modular Aero-Propulsion System Simulation (MAPSS). The goal of developing MAPSS was to have a flexible platform with easy access to engine, health, and control parameters. The model used was implemented using Simulink and compared to a previously developed model using FORTRAN. The Simulink environment was used because it provides a more user friendly platform.

MAPSS simulates a generic high pressure ratio, two-spool, low bypass military type engine with a digital controller [15]. The engine model is composed of the
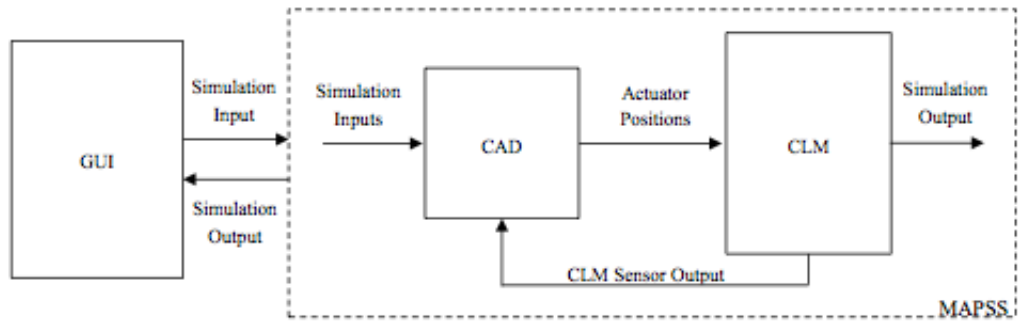
Figure 2.13: MAPSS Module Interaction Block Diagram (fom [15])

Controller and Actuator Dynamics (CAD) and Component Level Modules (CLM). Figure 2.13 shows how the GUI, CAD and CLM interact. The CAD block contains the controller sub-module that determines if the desired set points have been reached. The CLM block contains models of the individual components including the fan, booster, compressor, combustor, high pressure turbine (HPT), low pressure turbine (LPT), afterburner and nozzle. The user inputs the simulation parameters, including altitude, Mach number, and Power Lever Angle (PLA), in the GUI. Within the GUI, changes can be made to the controller, engine, and health parameters. After simulation, the outputs are sent to the GUI for examination.

To improve upon the efforts of MAPSS, NASA developed another engine simulation called Commercial Modular Aero-Propulsion System Simulation (C-MAPSS). This time the engine modeled is a 90,000 lb thrust class, two-spool, high bypass ratio commercial turbofan engine [8]. This type of engine has been used to study controls and health management. The engine is made up of a fan, low pressure compressor and low pressure turbine connected by the fan shaft. The high pressure compressor and high pressure turbine are connected by the core shaft. A diagram of the engine is shown in Figure 2.14.

The controller used in C-MAPSS was designed to represent a Full Authority Dig-
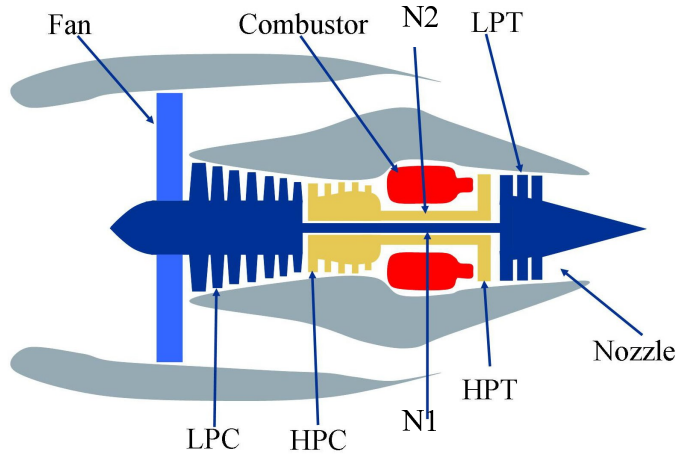
Figure 2.14: Diagram of 90k Engine (from [8])

ital Engine Controller (FADEC) that is commonly used on commercial aircrafts [3]. The control system contains a fan speed controller, four limit regulators and core speed acceleration and deceleration limiters implemented in a min-max scheme, shown in Figure 2.15. A gain scheduled linear control law is utilized for the fan speed (N_f) controller and each of the limit regulators. The individual control laws were designed using the model-matching, or KQ, method. The high limit regulator for the core speed (N_c) is implemented to avoid mechanical failure of the rotating components. The high pressure and high temperature components are protected by the high limits placed on the engine pressure ratio (epr) and the HPT outlet temperature $(T48)$. Lean combustor blowout is protected against with the implementation of a low limit on the burner static pressure $(Ps30)$. The purpose of the acceleration and deceleration limits is to prevent compressor stall during transients.

The capabilities of C-MAPSS provide a number of options for studying aircraft engine control. Linear engine models can be developed using open-loop simulation. The user can design linear point compensators and employ any self-designed controller within the C-MAPSS environment. There are 14 flight conditions included with the package, however, the user is able to add their own. The engine can be initialized
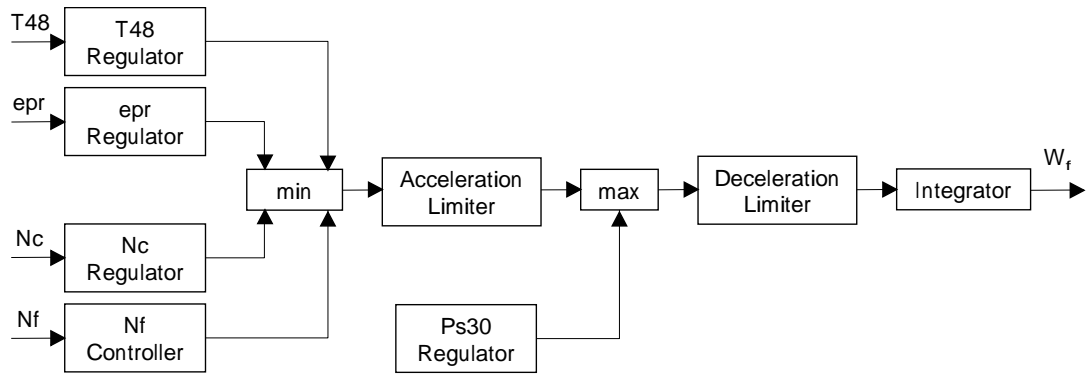
Figure 2.15: Overall Control Logic Block Diagram (from [8])

at any of these flight conditions and be used to generate linear point models that can then be used for analysis and design. The user is able to simulate the effects of deterioration by adjusting the health parameters.

A second version of C-MAPSS was developed with a few improvements on the original version. Sensor and actuator dynamics were included along with variable geometry effects and Reynolds' number effects. With these additions, changes had to be made to the gain scheduled controller, including the structure of the limit logic. The GUI was improved to streamline the functions of the simulations.

NASA has also developed the Commercial Modular Aero-Propulsion System Simulation 40k (C-MAPSS40k). In this latest installment, another generic commercial turbofan engine is used. This time the engine is capable of 35,000 lbf of thrust [14]. This version is capable of MIMO system simulation. Fuel flow rate (W_f), variable bleed valve position (VBV) and variable stator vane angle (VSV) can all be used to control the system, previously only W_f could be used. Simulation accuracy was increased by including a more precise steady-state operating point solver. The ability of the simulation to handle errors was improved. The user now has the option to use the GUI or the Matlab command line to interact with the system, easing operation on the user's end.

CHAPTER III

SLIDING MODE CONTROL

3.1   Introduction

Sliding mode control (SMC) is a control method that switches between two distinctly different control laws depending on the state of the system [5]. The system is forced to slide along a prescribed surface by the discontinuous control signal. This results in a robust control system. SMC is also advantageous because of its insensitivity to uncertain parameters and its ability to reject external disturbances. Once sliding mode has been reached, the system behaves as a reduced-order system. Chattering is an undesired characteristic of SMC systems that must be resolved.

3.2   Concept of Sliding Mode Control

There are a few key components of the sliding mode control system. First, the structure of the system is dictated by the sign of the function $s(x)$, the switching function, where x can be either a scalar or a vector. In the following discussion x is taken to be a scalar. The line on the phase plane described by $s(x) = 0$ is called the switching surface. There are three phases for the response of an SMC system. The first is the reaching mode. During the reaching condition, the initial state of the

system is driven toward the sliding surface. Next, the sliding mode occurs. The state slides along the sliding surface toward the equilibrium point. Lastly, the state reaches the equilibrium and this is called the steady-state mode.

There are two main steps to designing an SMC. First, the switching surface, $s(x) = 0$, must be designed so that the desired system dynamics are achieved. These trajectory dynamics are of a lower order than the given system dynamics. Next, a control law $u(x)$ must be designed to drive any initial state to the sliding surface in a finite amount of time.

Consider a SISO system represented by the equation

$$\dot{x} = Ax + Bu \tag{3.1}$$

The switching surface is chosen to be

$$s = Gx \tag{3.2}$$

During sliding mode $s = 0$. Substituting Equation 3.2 into $\dot{s} = 0$

$$
\begin{aligned}
\dot{s} &= G\dot{x} = 0 \\
&= G(Ax + Bu) = 0
\end{aligned}
\tag{3.3}
$$

Solving for u in Equation 3.3 the equivalent control, u_{eq}, can be found.

$$u_{eq} = \frac{-GAx}{GB} \tag{3.4}$$

This control can be plugged into Equation 3.1

$$
\begin{aligned}
\dot{x} &= Ax + Bu_{eq} \\
&= Ax - \frac{BGA}{GB}x \\
&= (A - \frac{BGA}{GB})x = A_{eq}x
\end{aligned}
\tag{3.5}
$$

If the matrix A_{eq} is Hurwitz, the sliding mode is stable. The values of the matrix G are chosen such that this is true.

In order to satisfy the reaching condition, the Lyapunov function approach is taken. The Lyapunov function candidate is chosen to be

$$V = \frac{1}{2}s^2 \tag{3.6}$$

In order to guarantee the reaching condition the following must be true.

$$\dot{V} = s\dot{s} < 0 \tag{3.7}$$

When the above statement is true, the value of s^2 goes to zero. Substituting $\dot{s} = G\dot{x}$ into Equation 3.7

$$\dot{V} = s\dot{s} = s(G\dot{x}) \tag{3.8}$$

From Equation 3.1 it is known that

$$s(G\dot{x}) = s(G(Ax + Bu)) \tag{3.9}$$

The control law is chosen to be

$$u = u_{eq} - \frac{\eta}{GB}sgn(s) \tag{3.10}$$

where u_{eq} comes from Equation 3.4 and η is the positive switching gain. Substituting Equation 3.10 into Equation 3.9 gives

$$
\begin{aligned}
\dot{V} &= s(GAx + GB(u_{eq} - \frac{\eta}{GB}sgn(s))) \\
&= s(GAx - GAx - \eta sgn(s)) \\
&= -\eta s sgn(s) \tag{3.11}
\end{aligned}
$$

Analyzing Equation 3.11, when $s > 0$, $sgn(s) = 1$, therefore $\dot{V} = -\eta s < 0$. When $s < 0$, $sgn(s) = -1$, therefore $\dot{V} = -\eta s < 0$. For any $s \neq 0$, $\dot{V}$ is always negative. This guarantees that the distance to the sliding surface $s = 0$ will always decrease.

3.3 Design Example

To better understand the concepts, an example from [9] is presented. A second order system is described by the following equations

$$\dot{x} = y$$
$$\dot{y} = 2y - x + u \tag{3.12}$$

The switching function, $s(x, y)$ is chosen to be

$$s(x, y) = x\sigma \tag{3.13}$$

where

$$\sigma = 0.5x + y$$

The control law is chosen to be

$$u = -\psi x \tag{3.14}$$

where

$$\psi = 4 \text{ when } s(x, y) > 0$$
$$= -4 \text{ when } s(x, y) < 0$$

The set of points where $s(x, y) = 0$ is known as the switching surface. To achieve this, either $x = 0$ or $s(x, y) = 0$. These lines are called the switching lines and are shown in Figure 3.1. Based on the sign of $s(x, y)$, the feedback gain, ψ, will switch giving two different system models. When $s(x, y) > 0$ (Region I), the model becomes

$$\dot{x} = y$$
$$\dot{y} = 2y - 5x \tag{3.15}$$

and when $s(x, y) < 0$ (Region II), the model becomes

$$\dot{x} = y$$
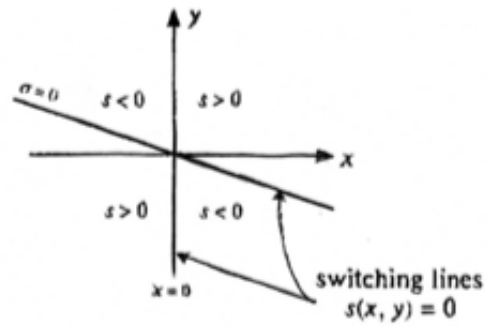$$\dot{y} = 2y + 3x \tag{3.16}$$

27

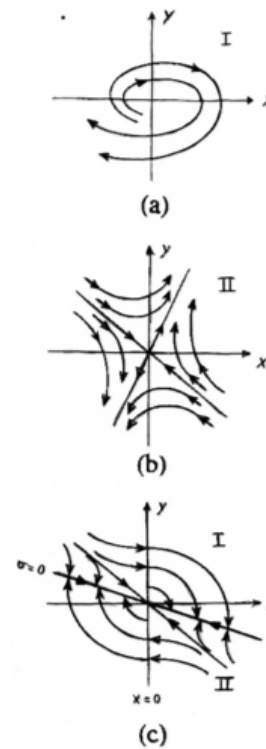Figure 3.1: Switching Lines on the Phase Plane

Figure 3.2: Phase Portraits

Figure 3.2 shows the phase plane trajectories of each of the models and the combined portrait where Regions I and II are defined by $x = 0$ and $\sigma = 0$. The phase trajectories consist of a reaching mode and a sliding mode. Starting from any point on the phase plane, the trajectory will move towards the switching lines. This is called the reaching mode. Once the switching line is reached, the trajectory will move towards the equilibrium, which in this case is the origin. The movement during sliding mode
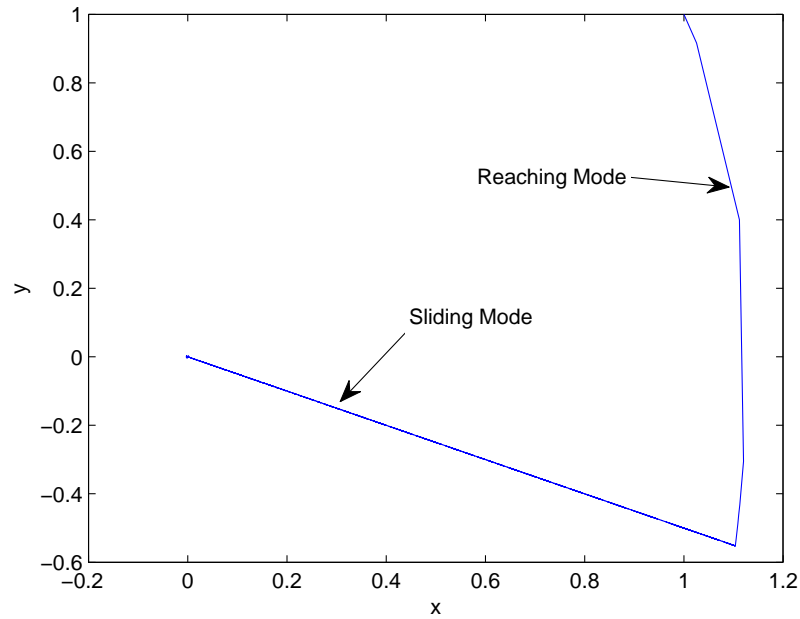
Figure 3.3: Trajectory Path of x vs. y

defines the transient response of the system. Also, during sliding mode the trajectory dynamics are of a reduced order from that of the original model, as shown in Equation 3.17.

$$\sigma = 0.5x + y = 0.5x + \dot{x} = 0 \tag{3.17}$$

It can be seen that the structure of the control system switches between the control law which is why this technique is also called variable structure control, however, many refer to it as sliding mode control to emphasize the role of the sliding mode.

A simulation of the SMC system was run to evaluate the controller. Figure 3.3 shows the trajectory starting from the initial conditions $x(0) = 1$ and $y(0) = 1$. It can be observed that the trajectory moves from the initial state towards the switching surface during the reaching phase. Once the surface is reached, the trajectory moves along the surface towards the equilibrium point, the origin. Figure 3.4 shows the switching function as it goes to $s = 0$ and stays on that line. Figure 3.5 shows the control action.
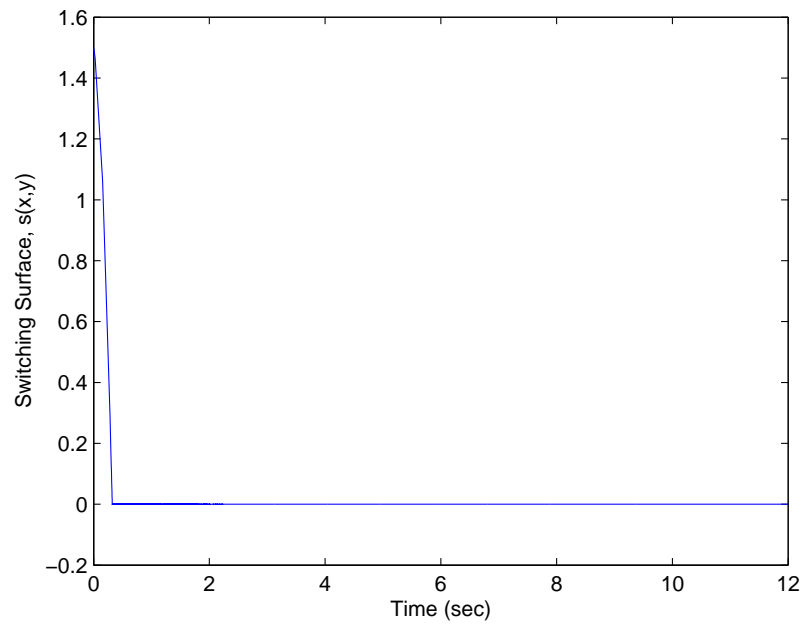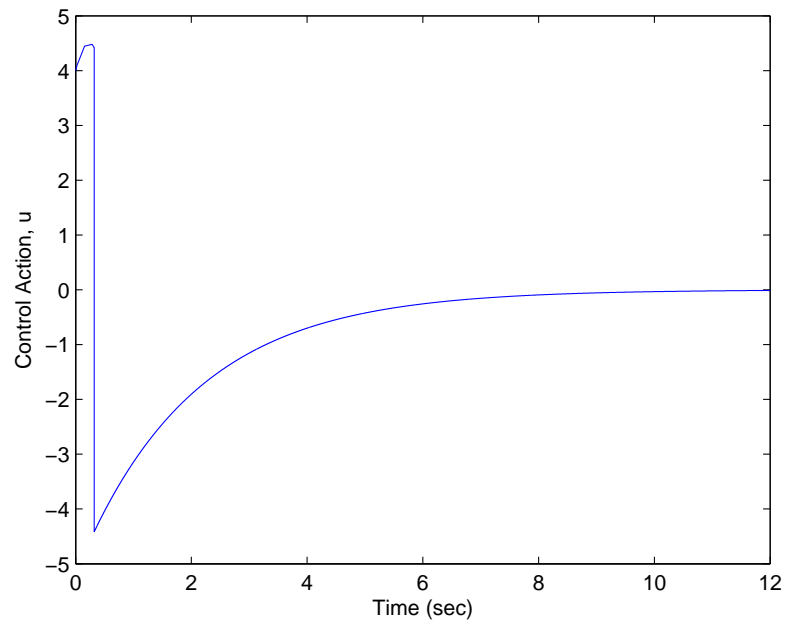
Figure 3.4: Switching Function vs. Time

Figure 3.5: Control Action vs. Time

3.4 Chattering Phenomenon

A major drawback of applying sliding mode control technique is the phenomenon of chattering. Chattering is motion which oscillates about the sliding surface [19]. Due to the discontinuous nature of the control that can occur during sliding mode, the switching of the control can excite unmodeled dynamics. Chattering is an undesirable characteristic of sliding mode control systems. It can cause wear of mechanical parts and high heat in power circuits [16].

One of the most common approaches to dealing with chatter is to apply a smooth approximation of $sgn(s)$ with a boundary layer approach. The $sgn(s)$ in Equation 3.18 is replaced with the saturation function, $sat(s)$, as shown in Equation 3.19.

$$u = \psi sgn(s) \tag{3.18}$$

$$u = \psi sat(s) \tag{3.19}$$

where

$$sat(s) = \begin{cases} 1, & s > L \\ \frac{s}{L}, & |s| \leq L \\ -1, & s < -1 \end{cases} \tag{3.20}$$

where $\pm L$ is the width of the boundary layer. The control is the same as relay control outside of the boundary layer. Inside of the boundary layer, the control is a linear feedback gain. However, if the slope in the middle of the approximation is too high, the unmodeled dynamics can be excited [17]. With the implementation of the boundary layer method, the ideal sliding mode does not occur. The trajectory is not forced to stay on $s = 0$.

CHAPTER IV

ADAPTIVE CONTROL

4.1 Introduction

The field of adaptive control came out of a desire to design autopilot systems for high-performance aircrafts in the 1950s [12]. Due to the changes in an aircraft's dynamics as it travels throughout its flight envelope, a constant-gain feedback control was not able to adequately control the aircraft. A controller that could adapt to these changes was necessary. A model reference adaptive control (MRAC) and an adaptive pole placement control were introduced. The first method that was used for designing the adaptive laws was the sensitivity method, including the MIT rule. Many lost interest in adaptive control because of a lack of understanding and a lack of stability proofs.

In the 1960s, adaptive control received a boost from the development of state space techniques and Lyapunov stability. The MIT rule was redesigned using the theory of Lyapunov stability. These advances, coupled with the developments in computers and electronics that were able to implement such complicated controllers, pushed adaptive control into the 1970s. MRAC schemes were redesigned with the Lyapunov approach and the concepts of positivity and hyperstability were developed and applied to a wide class of MRAC.

However, in the 1980s it was discovered that a system could go unstable if there were small disturbances or unmodeled dynamics. This led to the development of robust adaptive control. The robust adaptive controller was able to control a linear plant with unknown parameters. With the problem of robustness solved, the field moved toward focusing on performance. Adaptive control design was extended to nonlinear systems and there was an improvement in transient and steady-state control.

4.2   Adaptive Control

Adaptive control is made up of two parts: an on-line parameter estimator and a control law. The on-line parameter estimator, also called the adaptive law, estimates the unknown parameters at every instant. The control law is based on the known parameters of the system. The adaptive law may be applied directly or indirectly. Direct adaptive control uses the estimated parameters directly in the control law. For indirect adaptive control the estimated parameters are used to calculate the control parameters.

Model reference adaptive control (MRAC) stems from model reference control. In model referencing, the designer develops a model, the reference model, based on the plant and performance requirements that follows the properties of the closed-loop plant. The control law is developed so that the closed loop plant follows the dynamics of the reference model.

The key to adaptive control is the design of the adaptive law. The stability properties of the controller are based on the adaptive laws. Three methods for designing the adaptive law are the sensitivity method, positivity and Lyapunov design, and estimation of error cost criteria.

The sensitivity method was introduced in the 1960s and, although it has its drawbacks, it is still used to control uncertain plants in industrial applications [12]. In this

method the estimated parameters adjust so that a specified performance function is minimized. The partial derivative of the performance function with respect to the estimated parameters is multiplied by the error signal between the actual output and the desired. This partial derivative is referred to as the sensitivity function. The adaptive law is only implementable if this sensitivity function can be generated on-line. The main drawback of the sensitivity method is that in most cases this function can not be generated on-line. The MIT rule is a method that is used to approximate the sensitivity function [12]. The MIT rule replaces the unknown parameters that generate the sensitivity function with the parameters that are estimated on-line. Using an approximation can lead to weak stability properties and convergence of the tracking error can not be proven. However, simulations using the MIT rule showed that the performance was satisfactory if a small adaptive gain was used.

The lack of global stability in the sensitivity method led to research for new design methods. The Lyapunov design method applies the Lyapunov stability criteria and the relationship it has with positive real functions. The adaptive law is designed as a stability problem and the function is chosen so as to satisfy the Lyapunov criteria. This method is similar to the sensitivity method except, in this method, the functions can always be generated on-line. Another method is to choose a cost error function so that the sensitivity function is one that can be measured. The estimation error, the difference between the estimated and actual parameters, and the estimated parameters are set to be related in such a way that the cost function is decreasing. The approximate sensitivity functions can be generated from any number of cost criteria and methods, including gradient method and least-squares method.

4.3 Adaptive Sliding Mode Control

Proportional-integral-derivative (PID) control is commonly used throughout a wide range of controls engineering applications [13]. PID control is preferential due to its simple architecture and effectiveness. The key aspect of designing a PID controller is finding the values for the proportional gain, K_p, integral gain, K_i, and derivative gain, K_d. In typical PID control, these gains are usually fixed. However, an adaptive law has been developed [1] that is able to update the three parameters online during the control procedure.

Even though PID control is widely used throughout industrial application, it handles parameter variations and external disturbances poorly. As mentioned earlier, sliding mode control (SMC) is known for its robustness against these uncertainties. The SMC can be used as a supervisory controller along with the adaptive PID control [1]. Adding the SMC to the control scheme will enable the overall controller to adapt over time as well as reject external disturbances and protect against parameter variations.

4.4 Controller Design

Following the control design presented in [13] the uncertain second order system is shown below

$$
\begin{aligned}
\dot{x}_1(t) &= x_2(t) \\
\dot{x}_2(t) &= f(x_1, x_2, t) + \Delta f(x_1, x_2, t) + d(t) + bu \qquad (4.1) \\
y(t) &= x_1(t)
\end{aligned}
$$

where $x_1(t)$ and $x_2(t)$ are measurable states, u is the input, y is the output, b is the input gain, f is the nominal parameter of the plant, Δf is the plant uncertainty applied to the system, and $d(t)$ is the external disturbance applied to the system. The

error, e, is the difference between the desired trajectory, y_d, and the actual output, y.

$$e = y_d - y \tag{4.2}$$

The reference signal, x_r, is defined by

$$\dot{x}_r = \ddot{y}_d + K_1 \dot{e} + K_0 e \tag{4.3}$$

where K_1 and K_0 are chosen such that the roots of $s^2 + K_1 s + K_0 = 0$ are in the left-hand plane. The first step to designing the control law is to define the sliding surface as

$$\sigma = x_2 - x_r \tag{4.4}$$

When $\sigma = 0$, sliding mode occurs, hence

$$x_r = x_2 \tag{4.5}$$

Substituting Equation 4.5 into Equation 4.3

$$\ddot{e} + K_1 \dot{e} + K_0 e = 0 \tag{4.6}$$

This shows that as time goes to infinity the error will go to zero.

The next step is to determine the control law. Use the adaptive PID and SMC supervisory control

$$u = u_{pid} + u_s \tag{4.7}$$

where

$$u_{pid} = \frac{1}{b}(K_p e + K_i \int e \, dt + K_d \dot{e}) \tag{4.8}$$

$$u_s = -\frac{1}{b}(|f| + g + \alpha + |\dot{x}_r| + b|u_{pid}| + K_2) sgn(\sigma) \tag{4.9}$$

where g is a positive upper bound on Δf, $|\Delta f| \leq g$, and α is a positive upper bound on the disturbance, $|d(t)| \leq \alpha$. K_2 is a positive scalar gain. To ensure that the sliding

mode exists the sliding condition is derived using the Lyapunov stability theory. The Lyapunov function candidate is set to be

$$V = \frac{1}{2}\sigma^2 \tag{4.10}$$

The sliding condition is then

$$\dot{V} = \sigma\dot{\sigma} < 0 \tag{4.11}$$

When $\dot{V} < 0$ it is guaranteed that $\sigma \to 0$ as $t \to \infty$. From Equation 4.4

$$
\begin{aligned}
\dot{\sigma} &= \dot{x}_2 - \dot{x}_r \\
&= (f + \Delta f + d + bu) - \dot{x}_r \tag{4.12}
\end{aligned}
$$

Substituting Equation 4.12 into 4.11

$$
\begin{aligned}
\dot{V} &= \sigma[f + \Delta f + d + b(u_{pid} + u_s) - \dot{x}_r \tag{4.13}\\
&= [\sigma f - |\sigma||f|] + [\sigma\Delta f - |\sigma|g] + [\sigma d - |\sigma|\alpha] \\
&\quad + [b\sigma u_{pid} - b|\sigma||u_{pid}|] - [|\sigma||\dot{x}_r| + \sigma\dot{x}_r] - |\sigma|K_2 \\
&\leq [|\sigma||f| - |\sigma||f|] + [|\sigma||\Delta f| - |\sigma|g] + [|\sigma||d| - |\sigma|\alpha] \\
&\quad + [b|\sigma||u_{pid}| - b|\sigma||u_{pid}|] - [|\sigma||\dot{x}_r| + |\sigma||\dot{x}_r|] - |\sigma|K_2 \\
&< 0
\end{aligned}
$$

The adaptive laws for the control gains K_p, K_i, and K_d can be found using the gradient method and the chain rule on Equations 4.8 and 4.12.

$$\dot{K}_p = -\eta_1\frac{\partial\sigma\dot{\sigma}}{\partial K_p} = -\eta_1\frac{\partial\sigma\dot{\sigma}}{\partial u_{pid}}\frac{\partial u_{pid}}{\partial K_p} = -\eta_1\sigma e \tag{4.14}$$

$$\dot{K}_i = -\eta_2\frac{\partial\sigma\dot{\sigma}}{\partial K_i} = -\eta_2\frac{\partial\sigma\dot{\sigma}}{\partial u_{pid}}\frac{\partial u_{pid}}{\partial K_i} = -\eta_2\sigma\int edt \tag{4.15}$$

$$\dot{K}_d = -\eta_3\frac{\partial\sigma\dot{\sigma}}{\partial K_d} = -\eta_3\frac{\partial\sigma\dot{\sigma}}{\partial u_{pid}}\frac{\partial u_{pid}}{\partial K_d} = -\eta_1\sigma\dot{e} \tag{4.16}$$

where η_i is a positive learning rate. Proper selection of the learning rates and the initial values of the control gains is important. However, the use of the supervisory

controller provides a backup that will help pull the states back if they begin to diverge [1].

To deal with the phenomenon of chattering, the boundary layer technique is applied. The $sgn(\sigma)$ in Equation 4.9 is replaced with the saturation function, $sat(\frac{\sigma}{\delta})$, where

$$sat(\frac{\sigma}{\delta}) = \begin{cases} 1, & \frac{\sigma}{\delta} \geq 1 \\ \frac{\sigma}{\delta}, & -1 < \frac{\sigma}{\delta} < 1 \\ -1, & \frac{\sigma}{\delta} \leq -1 \end{cases} \qquad (4.17)$$

where δ is the width of the boundary layer.

CHAPTER V

IMPLEMENTATION AND

SIMULATION

5.1 Introduction

In this chapter, the adaptive PID sliding mode control (A-SMC) is applied to the aircraft engine. An A-SMC is developed for each of the following: (1) fan speed (N_f) controller, (2) engine pressure ratio (epr) limit regulator, (3) high pressure turbine exit temperature ($T48$) limit regulator, (4) core speed (N_c) limit regulator, and (5) burner static pressure ($Ps30$) limit regulator. The five A-SMC are then implemented into the min-max structure in the C-MAPSS environment. Three different simulations are run to test the adaptability and robustness of the overall controller.

5.2 Implementation

5.2.1 Fan Speed Controller

The first step to designing the fan speed controller is to find the transfer function for fan speed to fuel flow. This can be found in C-MAPSS by creating the linear engine model at a desired flight condition and converting the state space equations

to a transfer function. Flight Condition 01 [8] is arbitrarily chosen as the point for finding this transfer function. The equilibrium values at Flight Condition 01 can be found in the Appendix.

$$G_{N_f}(s) = \frac{230.7s + 2032}{s^2 + 8.564s + 17.47} \tag{5.1}$$

In order to use the A-SMC method as presented in [13] the zero of the transfer function is ignored for the sake of design. It will be included during the simulation. This gives the transfer function

$$G_{N_f d}(s) = \frac{2032}{s^2 + 8.564s + 17.47} \tag{5.2}$$

From here, the equation can be expressed as a second-order system

$$
\begin{aligned}
\dot{x}_1 &= x_2 \\
\dot{x}_2 &= -8.564x_2 - 17.47x_1 + 2032u \\
y &= x_1
\end{aligned}
\tag{5.3}
$$

where the states x_1 and x_2 are ΔN_f and $\dot{N}_f$ respectively. The control input u is ΔW_f.

The structure of the fan speed controller can be established. A diagram is shown in Figure 5.1. The designer selected variables can be found in the Appendix. The variables g and α have both been set to zero for simplification.

The diagram in Figure 5.2 shows the reference generator equation. Figure 5.3 shows the layout of the adaptive PID controller and the diagram of the adaptive gain laws is shown in Figure 5.4. The sliding mode controller is shown in Figure 5.5.

Figure 5.1: Diagram of Fan Speed Controller
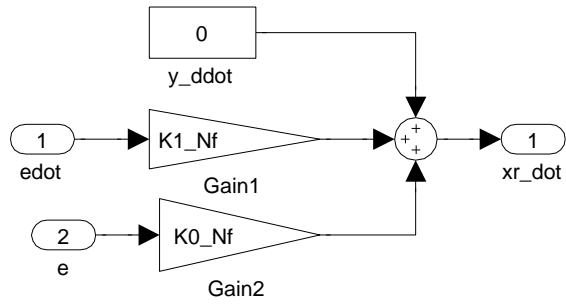
Figure 5.2: Diagram of Fan Speed Reference Generator
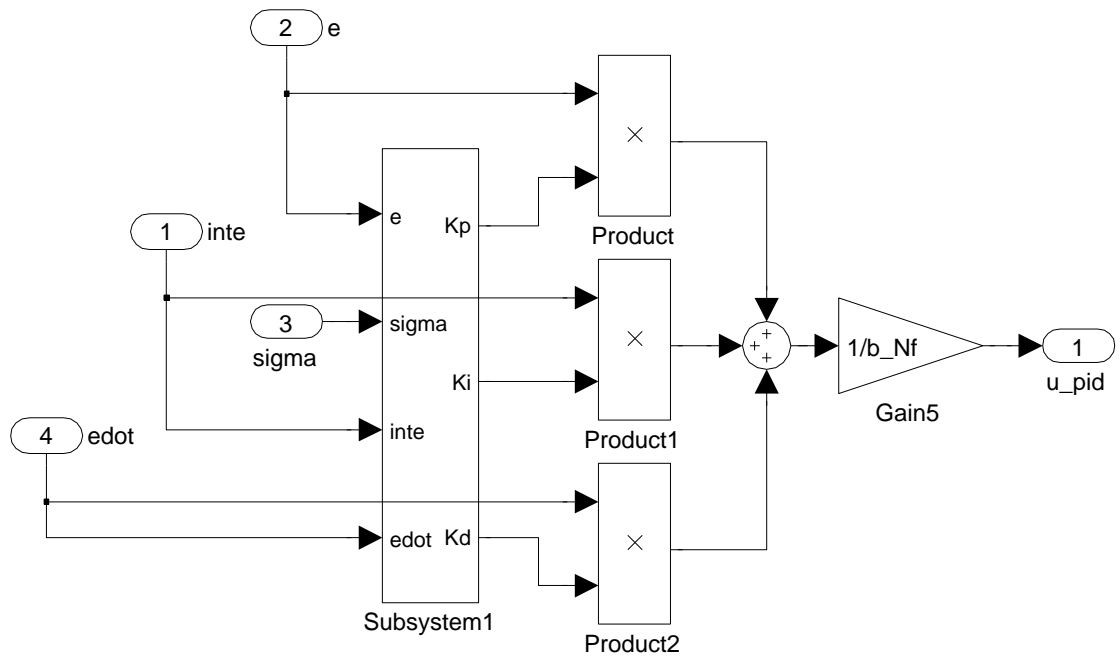
Figure 5.3: Diagram of Fan Speed Adaptive PID Control
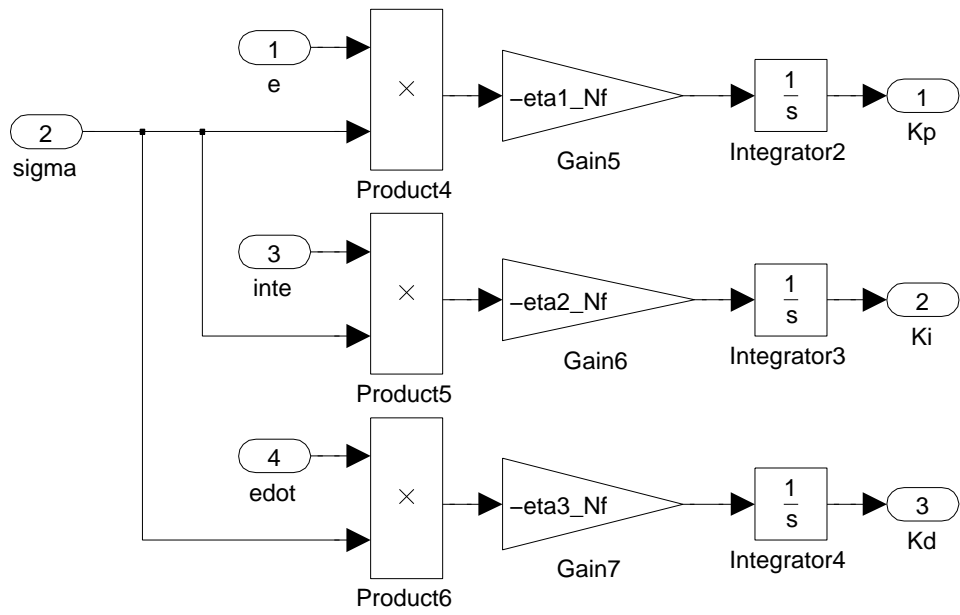
Figure 5.4: Diagram of Adaptive PID Gain Laws
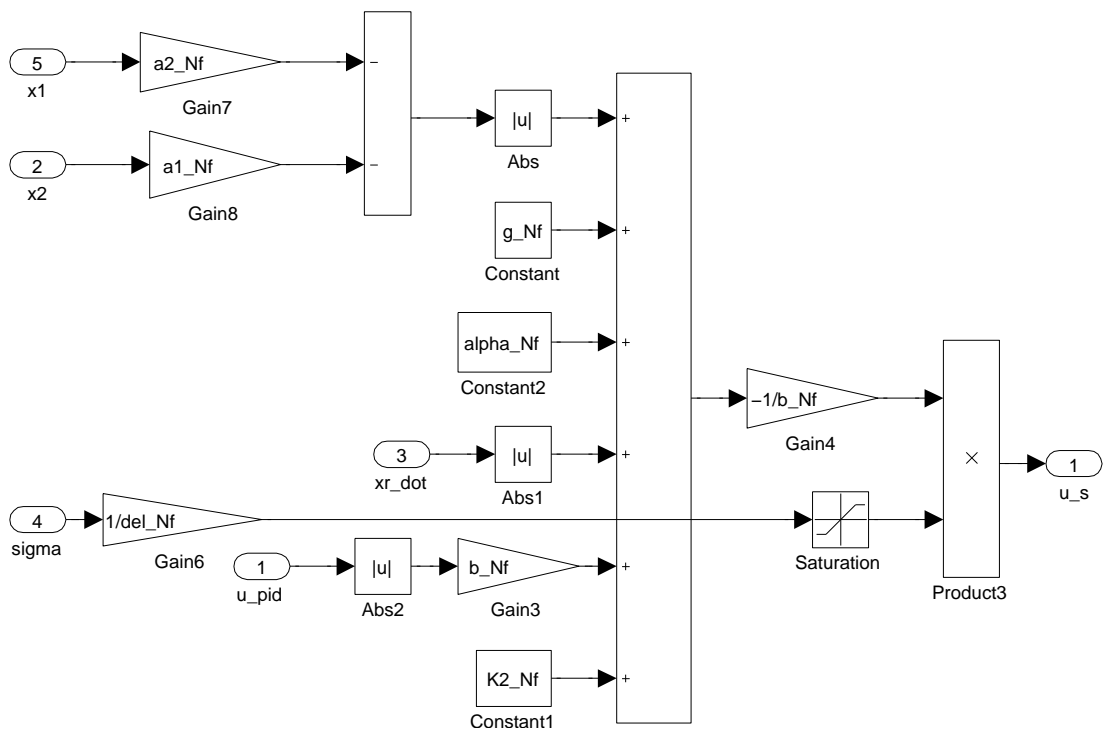
Figure 5.5: Diagram of Fan Speed SMC Control

5.2.2 Engine Pressure Ratio Limit Regulator

Designing the limit regulators follows the same methodology as was used to design the fan speed controller. The transfer function for engine pressure ratio to fuel flow is found in C-MAPSS at Flight Condition 01 [8].

$$G_{epr}(s) = \frac{0.02364s^2 + 0.343s + 1.026}{s^2 + 8.564s + 17.47} \tag{5.4}$$

The zeros of the transfer function are ignored. The design transfer function is

$$G_{eprd}(s) = \frac{1.026}{s^2 + 8.564s + 17.47} \tag{5.5}$$

This equation can be written as a second order system.

$$
\begin{aligned}
\dot{x}_1 &= x_2 \\
\dot{x}_2 &= -8.564x_2 - 17.47x_1 + 1.026u \\
y &= x_1
\end{aligned}
\tag{5.6}
$$

where x_1 and x_2 are Δepr and $\frac{d}{dt}epr$. Again, the control input u is ΔW_f. A diagram of the structure of this limit regulator is shown in Figure 5.6. The designer selected variables are shown in the Appendix.

Figure 5.6: Diagram of Engine Pressure Ratio Limit Regulator

5.2.3 High Pressure Turbine Exit Temperature Limit Regulator

The transfer function for HPT exit temperature to fuel flow is found in C-MAPSS at Flight Condition 01 [8].

$$G_{T48}(s) = \frac{146.4s^2 + 1030s + 1595}{s^2 + 8.564s + 17.47} \tag{5.7}$$

The zeros of the transfer function are ignored. The design transfer function is

$$G_{T48d}(s) = \frac{1595}{s^2 + 8.564s + 17.47} \tag{5.8}$$

This equation can be written as a second order system.

$$
\begin{aligned}
\dot{x}_1 &= x_2 \\
\dot{x}_2 &= -8.564x_2 - 17.47x_1 + 1595u \\
y &= x_1
\end{aligned}
\tag{5.9}
$$

where the states x_1 and x_2 are $\Delta T48$ and $\frac{d}{dt}T48$. The control input u is ΔW_f. A diagram of the structure of this limit regulator is shown in Figure 5.7. The designer selected variables are shown in the Appendix.
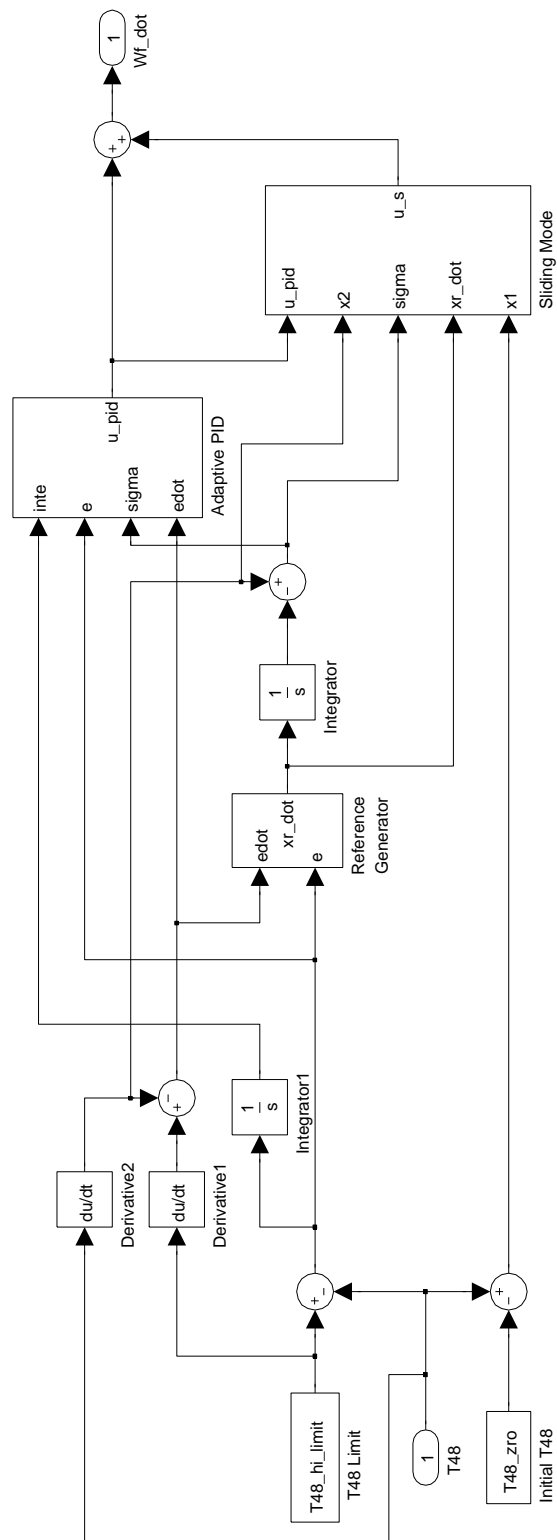
Figure 5.7: Diagram of HPT Exit Temperature Limit Regulator

5.2.4 Core Speed Limit Regulator

The transfer function for core speed to fuel flow is found in C-MAPSS at Flight Condition 01 [8].

$$G_{N_c}(s) = \frac{653.6s + 2628}{s^2 + 8.564s + 17.47} \tag{5.10}$$

The zero of the transfer function is ignored. The design transfer function is

$$G_{N_cd}(s) = \frac{2628}{s^2 + 8.564s + 17.47} \tag{5.11}$$

This equation can be written as a second order system.

$$
\begin{aligned}
\dot{x}_1 &= x_2 \\
\dot{x}_2 &= -8.564x_2 - 17.47x_1 + 2628u \\
y &= x_1
\end{aligned}
\tag{5.12}
$$

where the states x_1 and x_2 are ΔN_c and $\dot{N}_c$. The control input u is ΔW_f. A diagram of the structure of this limit regulator is shown in Figure 5.8. The designer selected variables are shown in the Appendix.

Figure 5.8: Diagram of Core Speed Limit Regulator

5.2.5 Burner Static Pressure Limit Regulator

The transfer function for burner static pressure to fuel flow is found in C-MAPSS at Flight Condition 01 [8].

$$G_{Ps30}(s) = \frac{20.11s^2 + 309.5s + 962}{s^2 + 8.564s + 17.47} \qquad (5.13)$$

The zeros of the transfer function are ignored. The design transfer function is

$$G_{Ps30d}(s) = \frac{962}{s^2 + 8.564s + 17.47} \qquad (5.14)$$

This equation can be written as a second order system.

$$
\begin{aligned}
\dot{x}_1 &= x_2 \\
\dot{x}_2 &= -8.564x_2 - 17.47x_1 + 962u \qquad (5.15) \\
y &= x_1
\end{aligned}
$$

where the states x_1 and x_2 are $\Delta Ps30$ and $\frac{d}{dt}Ps30$. The control input u is ΔW_f. A diagram of the structure of this limit regulator is shown in Figure 5.9. The designer selected variables are shown in the Appendix.
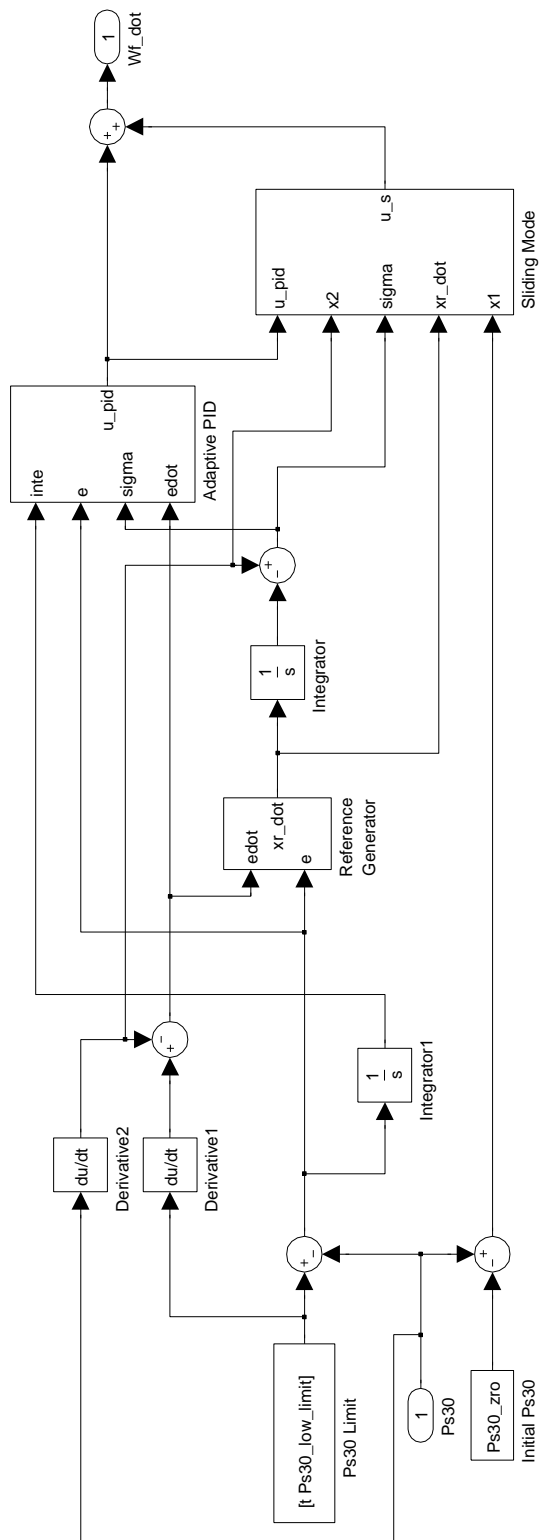
Figure 5.9: Diagram of Burner Static Pressure Limit Regulator

5.2.6 Min-Max Selection

The fan speed controller and four limit regulators are placed in a min-max scheme as shown in Figure 5.10. The outputs of the fan speed (N_f) controller and the HPT exit temperature ($T48$), engine pressure ratio (epr), and core speed (N_c) limit regulators are compared and the minimum is passed through the minimum block. This signal is then passed into the acceleration limiter. The output of the acceleration limiter is compared to the output of the burner static pressure ($Ps30$) limit regulator in the maximum block. This output is passed into the deceleration limiter and the final output, $\dot{W}_f$, is passed through a free integrator to get the control signal, fuel flow (W_f). The free integrator allows the control signals to be calculated as incremental commands.
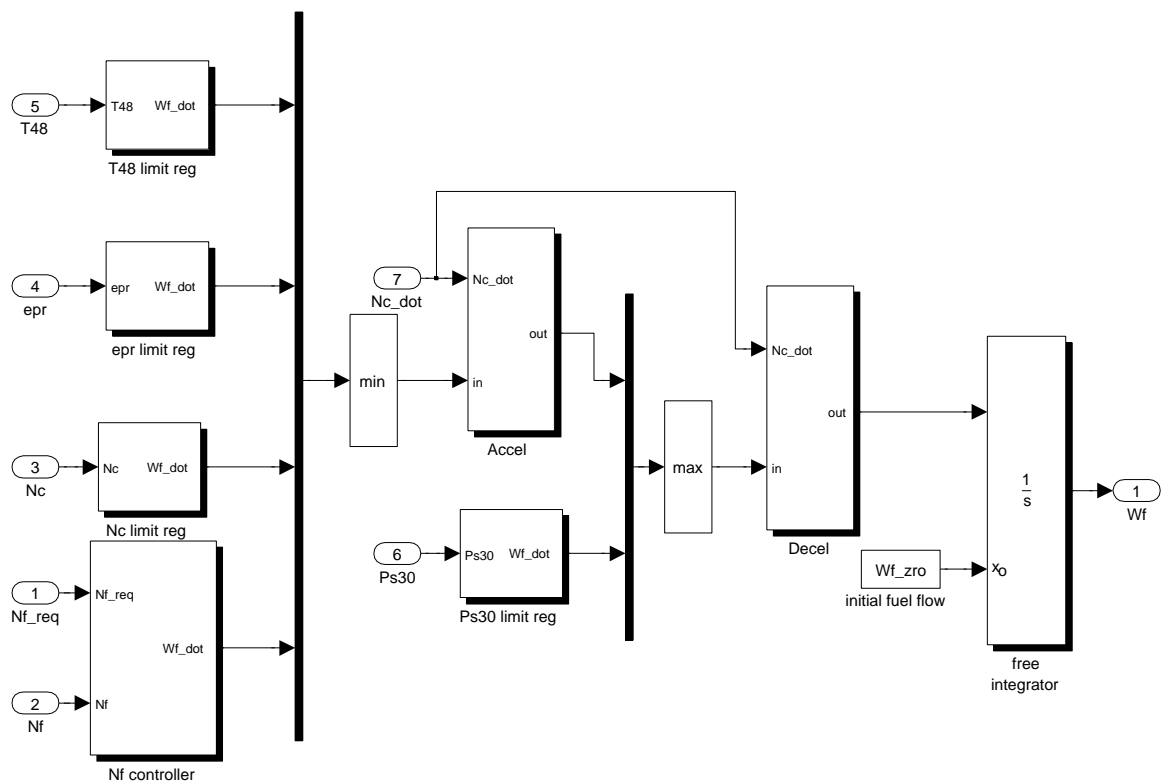
Figure 5.10: Diagram of Min-Max Selection

5.3   Simulation

The complete adaptive PID sliding mode controller has been simulated in the
C-MAPSS environment. The adaptability and robustness are evaluated for three
prescribed functions of time from [8].

5.3.1   Burst and Chop

The first simulation is a maneuver called burst and chop. The user inputs for
C-MAPSS are altitude, Mach number, sea-level temperature, and throttle resolver
angle (TRA) and are shown in Figure 5.11.

- Altitude: sea level (constant)

- Mach Number: static (constant)

- Sea Level Temperature: $59\,{}^{\circ}F$ (constant)

- TRA: 20° ($t = 0 : 2$ sec), 100° ($t = 2.5 : 15$ sec), 20° ($t = 15.5 : 25$ sec)

The results of the simulation are shown in Figures 5.12 through 5.16. Figure 5.12
shows the fan speed response of the A-SMC controller. The A-SMC controller is able
to follow the demanded fan speed. The limit regulators are shown in Figures 5.13
through 5.16. It is shown that the limits are not violated except, briefly, the *epr* limit
is exceeded but then slides along the limit. This shows that the engine is operating
at one of the limits so that it can obtain maximum power during a large transient.
A comparison of the fuel flow rate of the A-SMC controller and of the C-MAPSS
controller (KQ) is shown in Figure 5.17. The fuel flow rates are similar which leads
to little improvement in the engine response. Figure 5.18 shows that the switching
function of the fan speed controller goes to zero when the system has settled. Finally,
the adaptive gains for each A-SMC are given in Figures 5.19 through 5.23. The gains
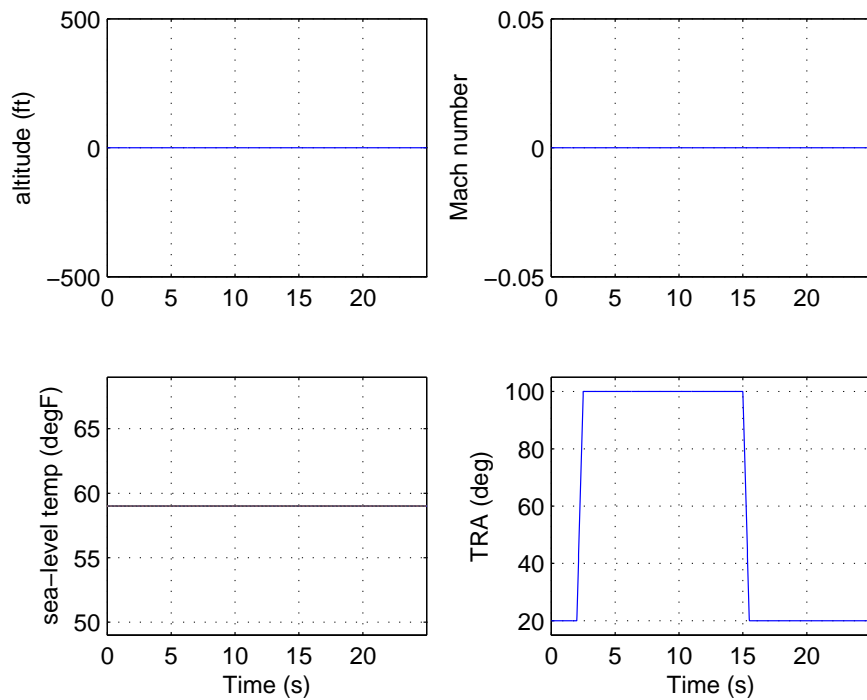
Figure 5.11: User Inputs for Burst and Chop

for the fan speed all adapt. However, when the engine is operating away from its limits there is a large error between the limit and the actual value. This causes the values for K_p and K_i to continue to increase. The values for K_d level off because the derivative of the error goes to zero. This can cause problems during actual flight because the length of a flight is considerably longer than the 25 sec used for the simulations. If the gains are too high, they may not be able to adapt quickly enough to changes in flight conditions.
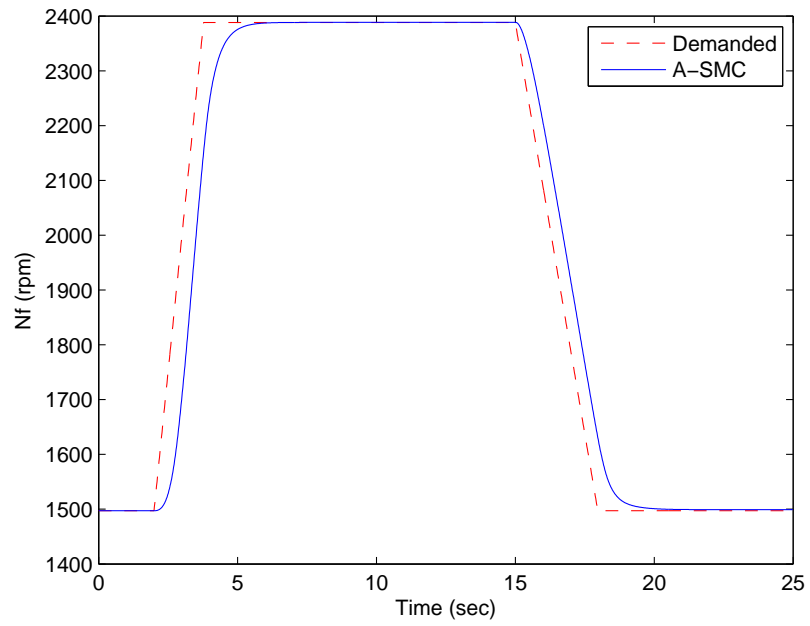
Figure 5.12: Fan Speed (N_f) vs Time for Burst and Chop
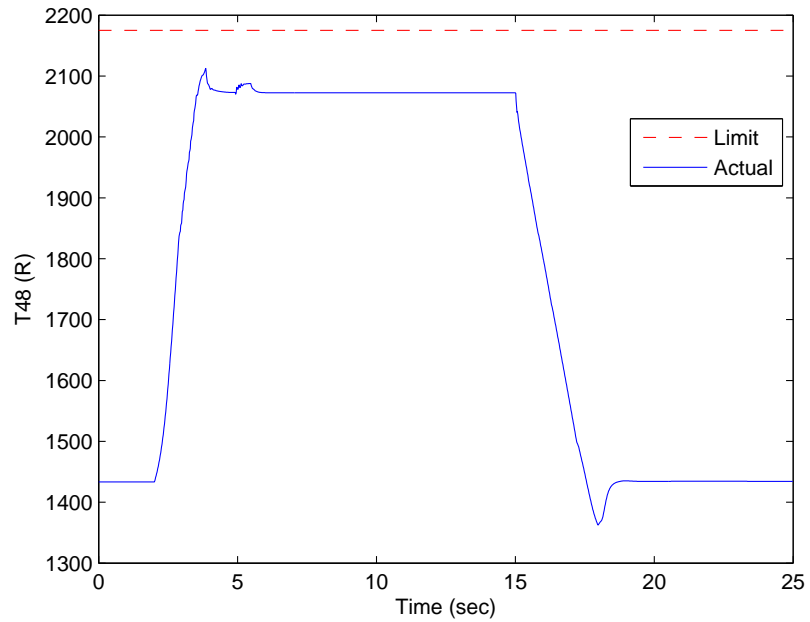
Figure 5.13: HPT Exit Temp ($T48$) vs Time for Burst and Chop

55
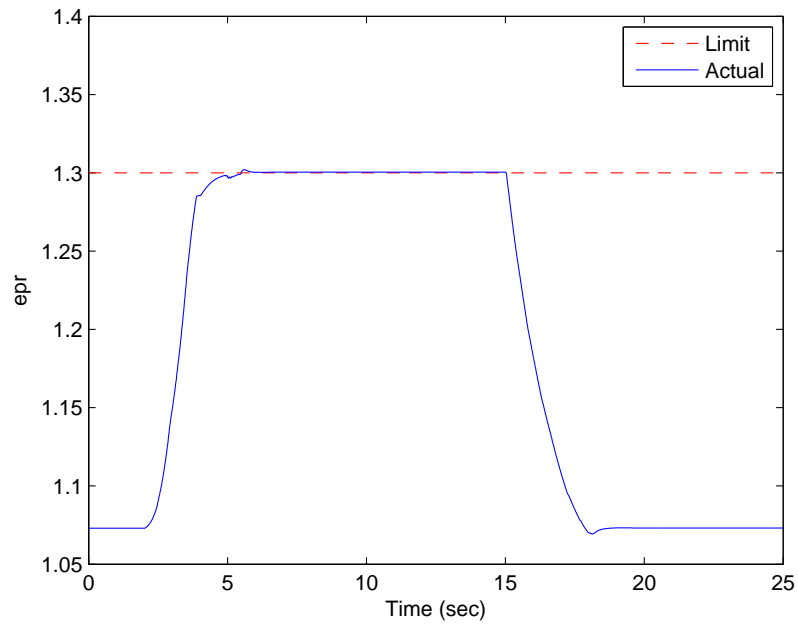
Figure 5.14: Engine Pressure Ratio (epr) vs Time for Burst and Chop
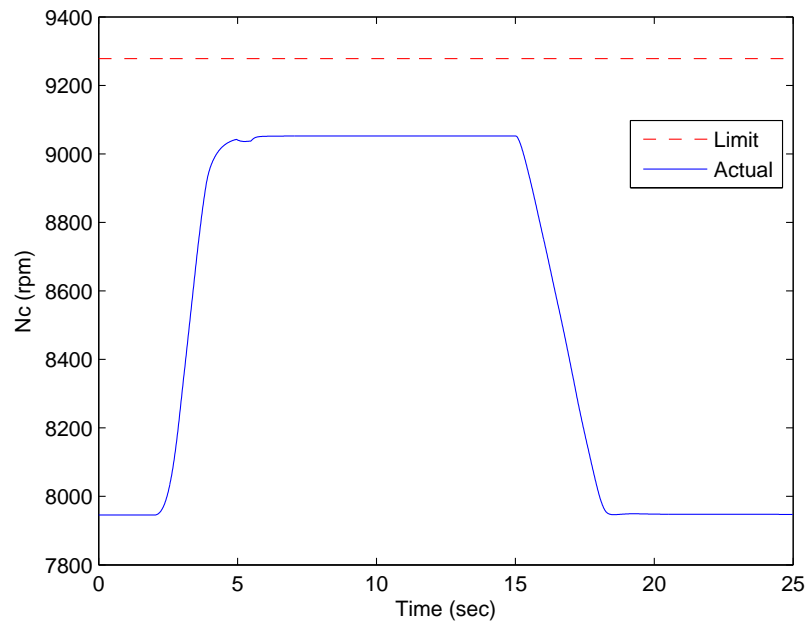
Figure 5.15: Core Speed (N_c) vs Time for Burst and Chop
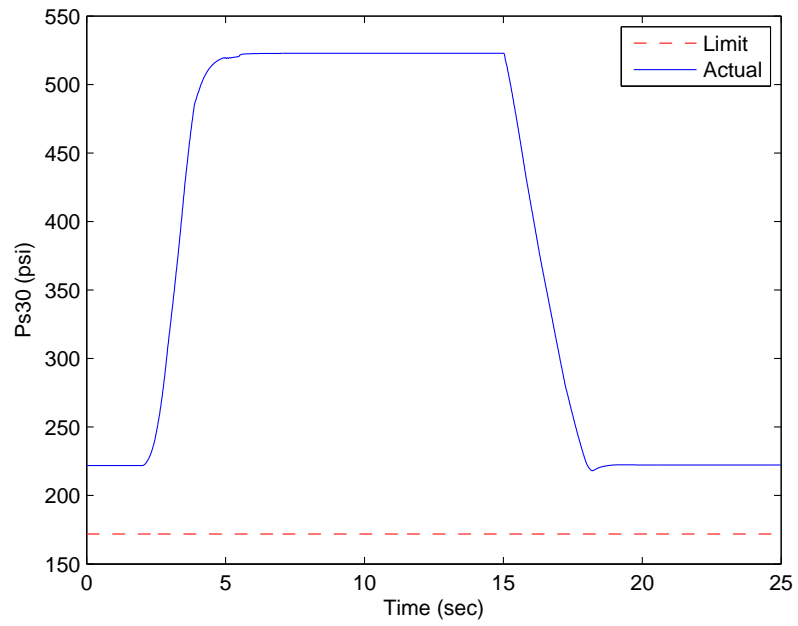
Figure 5.16: Burner Static Pressure ($Ps30$) vs Time for Burst and Chop
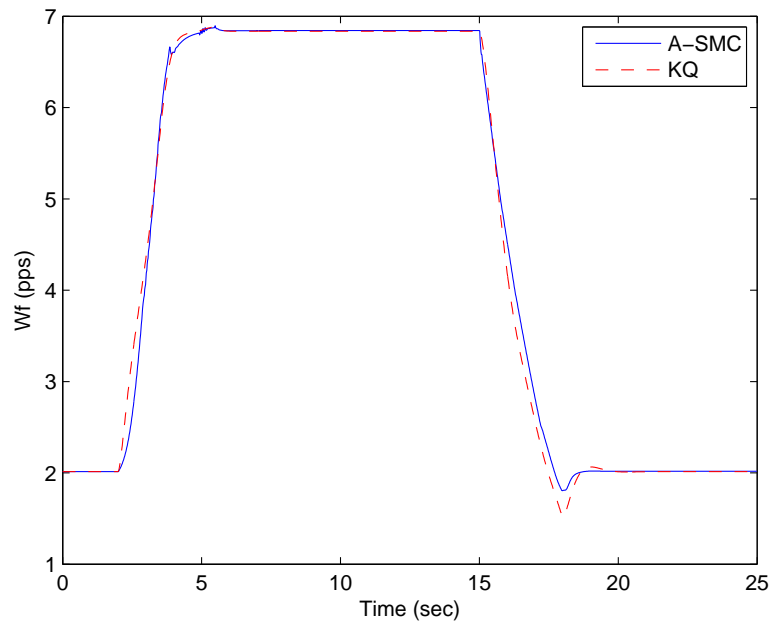
Figure 5.17: Fuel Flow (W_f) vs Time for Burst and Chop
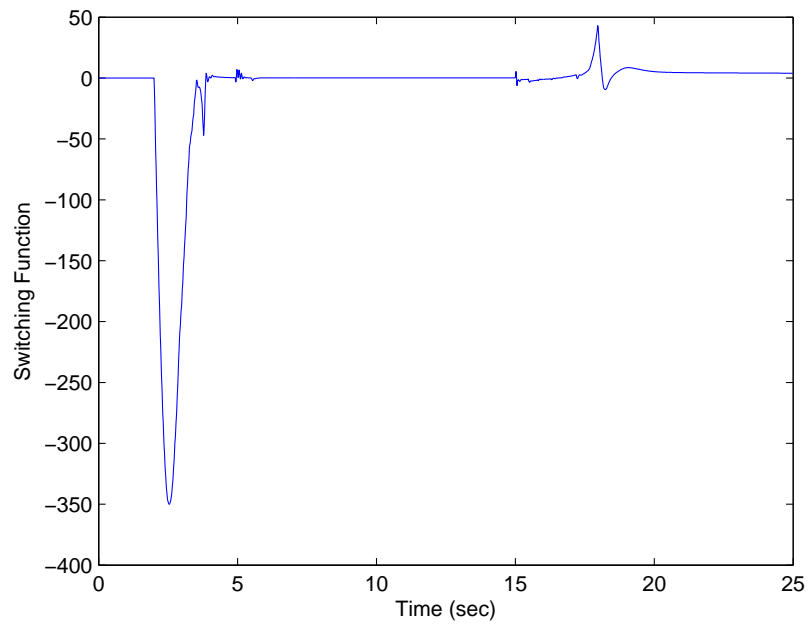
Figure 5.18: Fan Speed σ vs Time for Burst and Chop
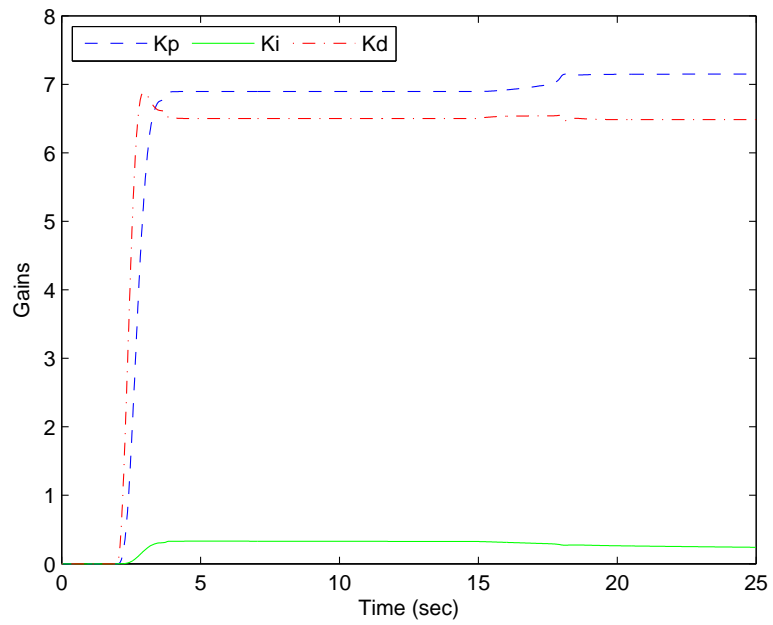
Figure 5.19: Fan Speed Adaptive Gains vs Time for Burst and Chop
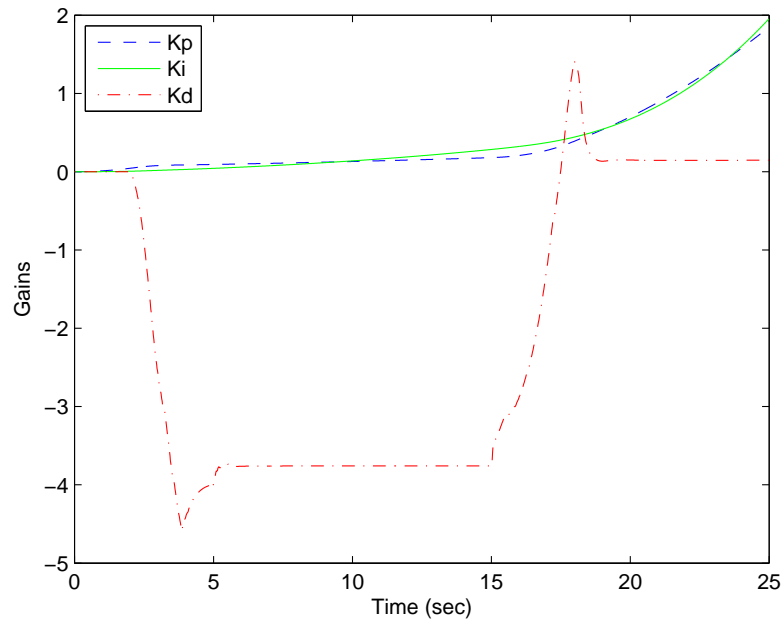
Figure 5.20: HPT Exit Temp Adaptive Gains vs Time for Burst and Chop
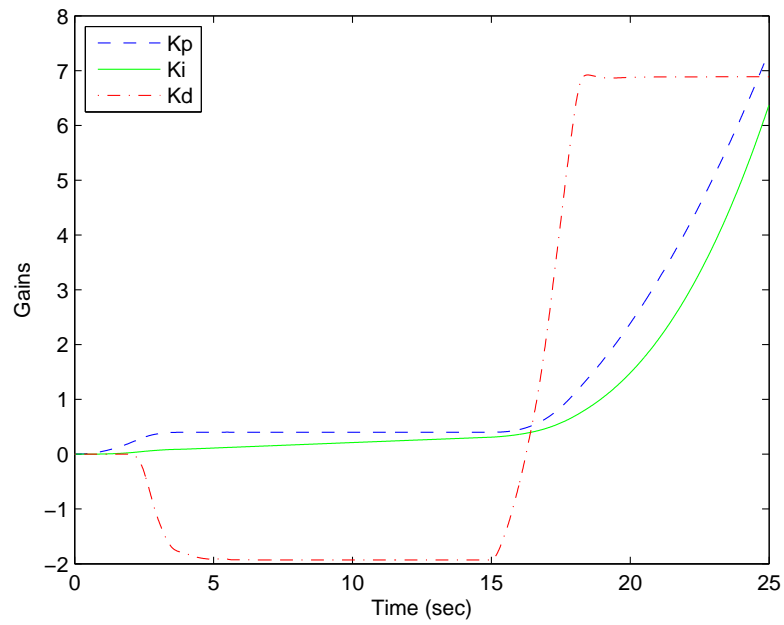
Figure 5.21: Engine Pressure Ratio Adaptive Gains vs Time for Burst and Chop
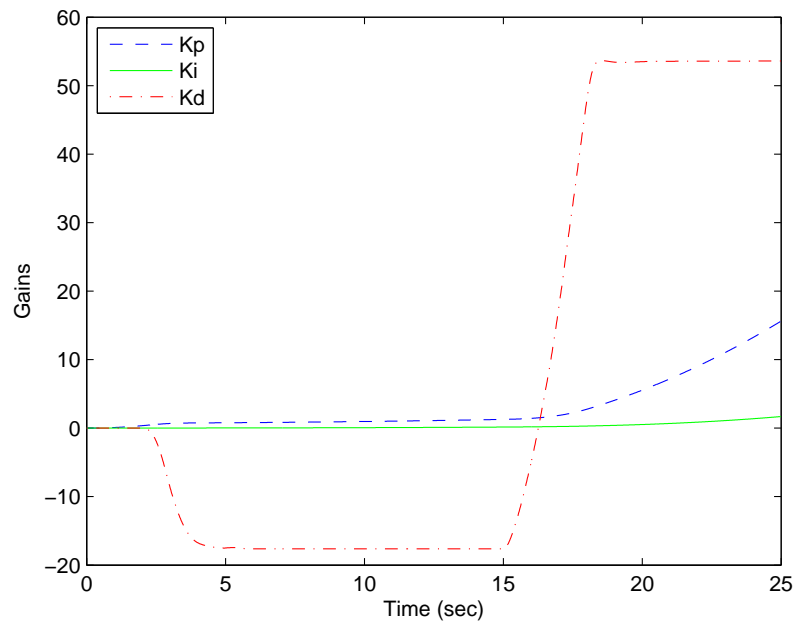
Figure 5.22: Core Speed Adaptive Gains vs Time for Burst and Chop
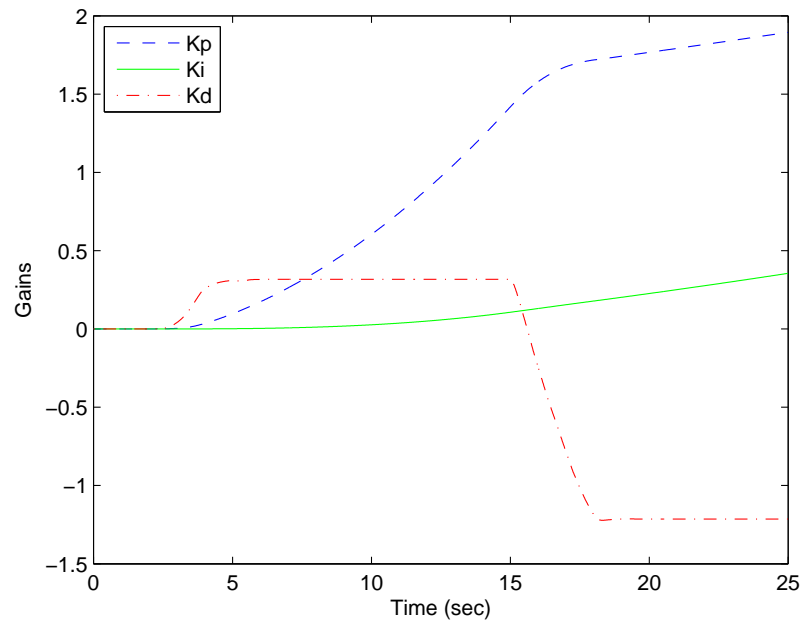
Figure 5.23: Burner Static Pressure Adaptive Gains vs Time for Burst and Chop

60

5.3.2 Long Descent

The second simulation is of a long descent. The user inputs for C-MAPSS are shown in Figure 5.24.

- Altitude (feet): 42,000 ($t = 0 : 2$ sec), 40,000 ($t = 9 : 12$ sec), 0 ($t = 22 : 25$ sec)

- Mach Number: 0.84 ($t = 0 : 2$ sec), 0.7 ($t = 9 : 12$ sec), 0.2 ($t = 22 : 25$ sec)

- Sea Level Temperature: 59 $^\circ F$ (constant)

- TRA: 100° ($t = 0 : 2$ sec), 60° ($t = 9 : 25$ sec)

The results of the simulation are shown in Figures 5.25 through 5.36. Figure 5.25 shows the fan speed response of the A-SMC controller. The A-SMC controller is able to follow the demanded fan speed. The limit regulators are shown in Figures 5.26 through 5.29. It is shown that the limits are not exceeded. None of the limits
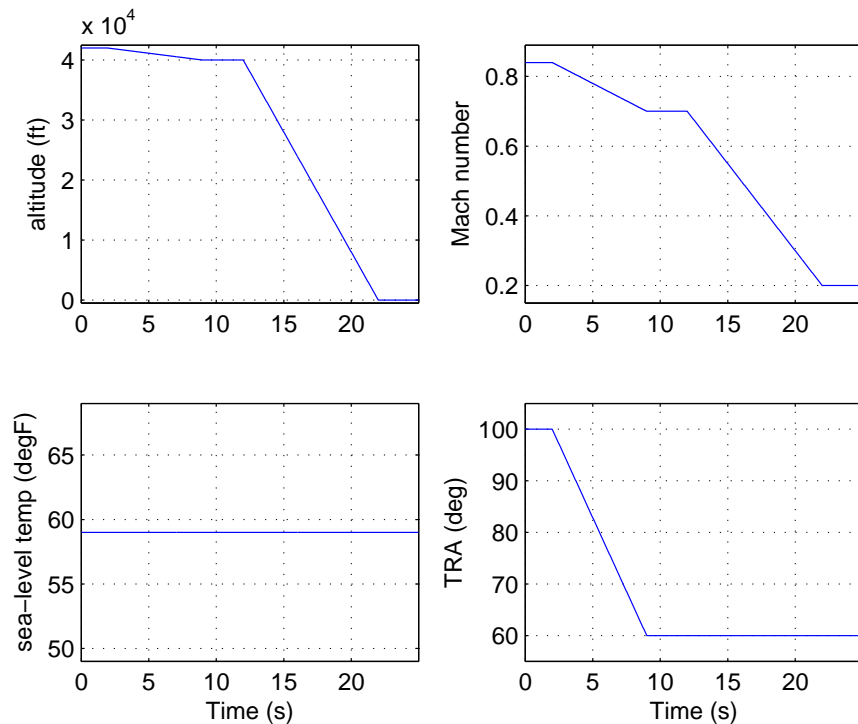
Figure 5.24: User Inputs for Long Descent
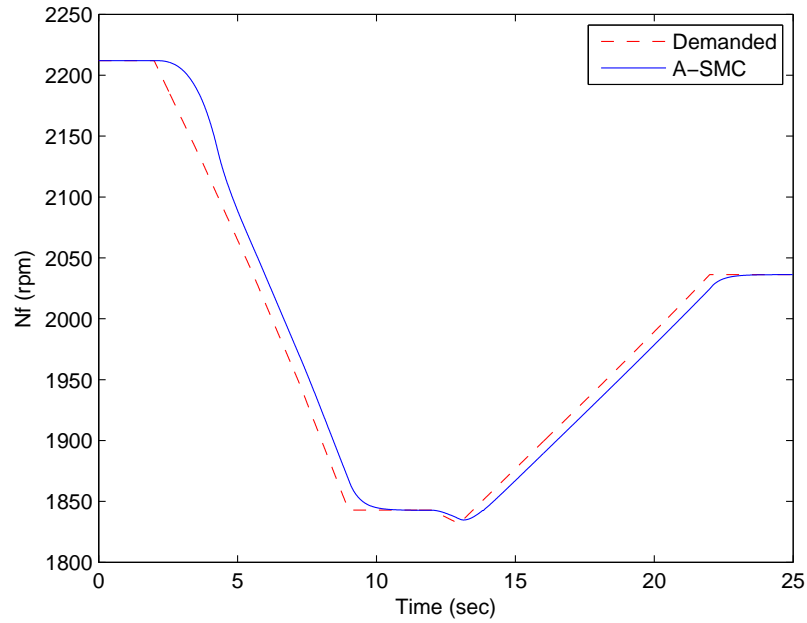
Figure 5.25: Fan Speed (N_f) vs Time for Long Descent

are reached because the engine does not have a need to operate at maximum power. A comparison of the fuel flow rate of the A-SMC controller and of the C-MAPSS controller (KQ) is shown in Figure 5.30. The fuel flow from the A-SMC controller rises more quickly than the KQ controller after $t = 15$ sec. This results in better fan speed response. However, this still does not provide a drastic improvement in engine performance. Figure 5.31 shows the switching function of the fan speed controller goes to zero when the system has settled. Finally, the adaptive gains for each A-SMC are given in Figures 5.32 through 5.36. Again, it is shown that the gains for the fan speed controller are able to adapt while the values of K_p and K_i for the limit regulators continuously increase. The K_d gains for the limit regulators level off because the derivative of the errors goes to zero.
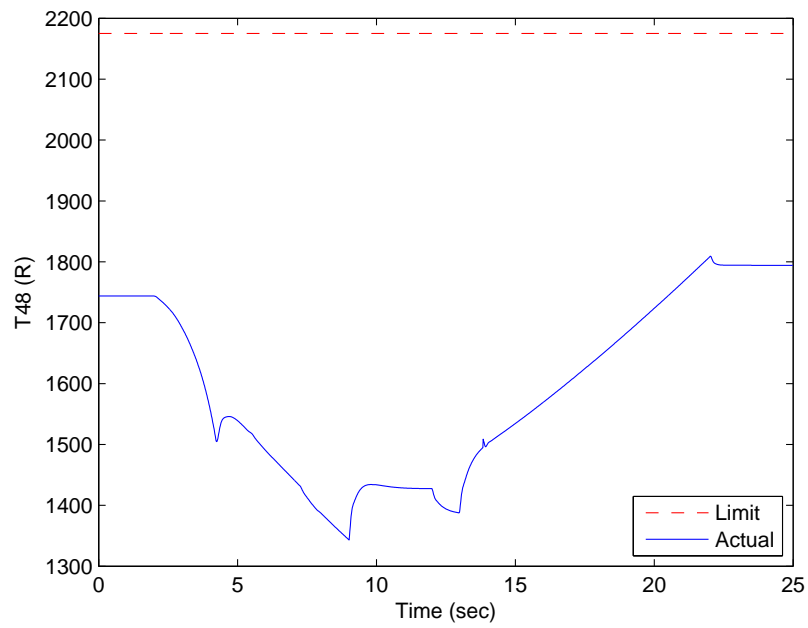
Figure 5.26: HPT Exit Temp ($T48$) vs Time for Long Descent
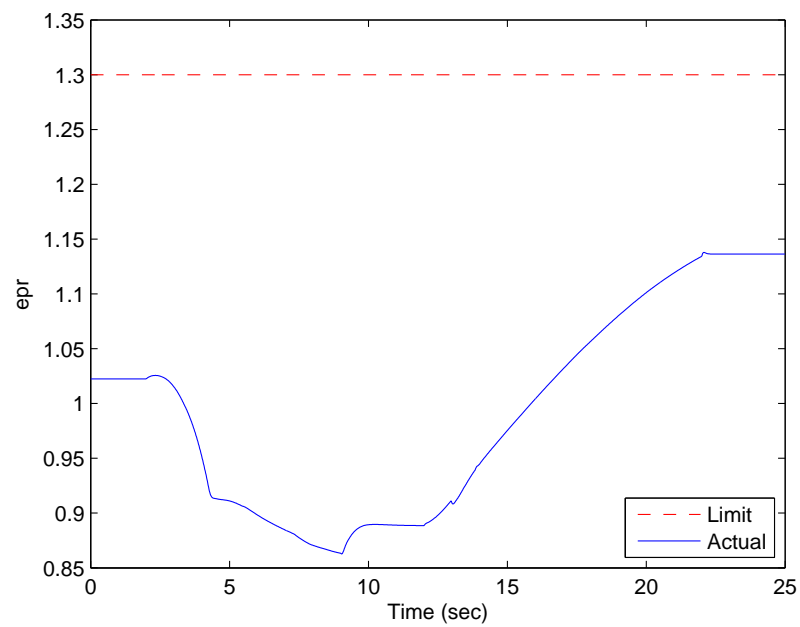
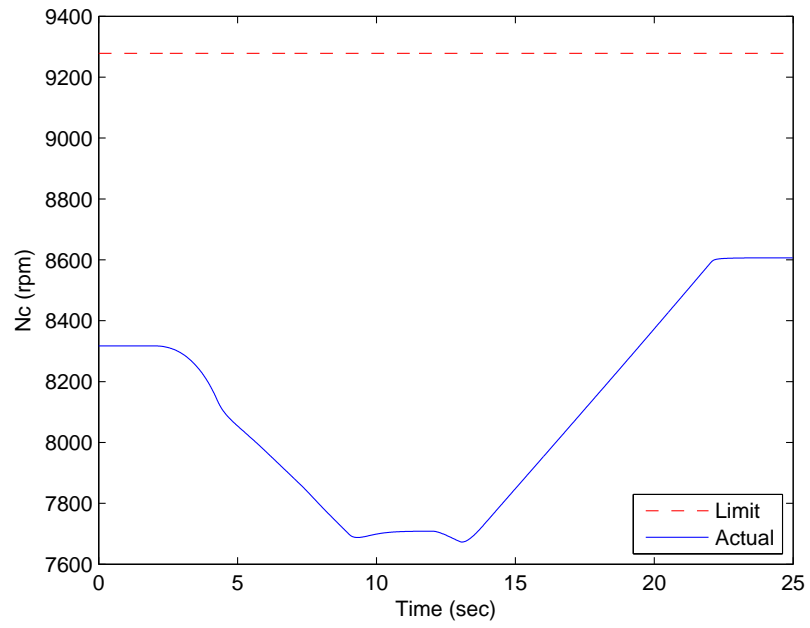Figure 5.27: Engine Pressure Ratio (epr) vs Time for Long Descent

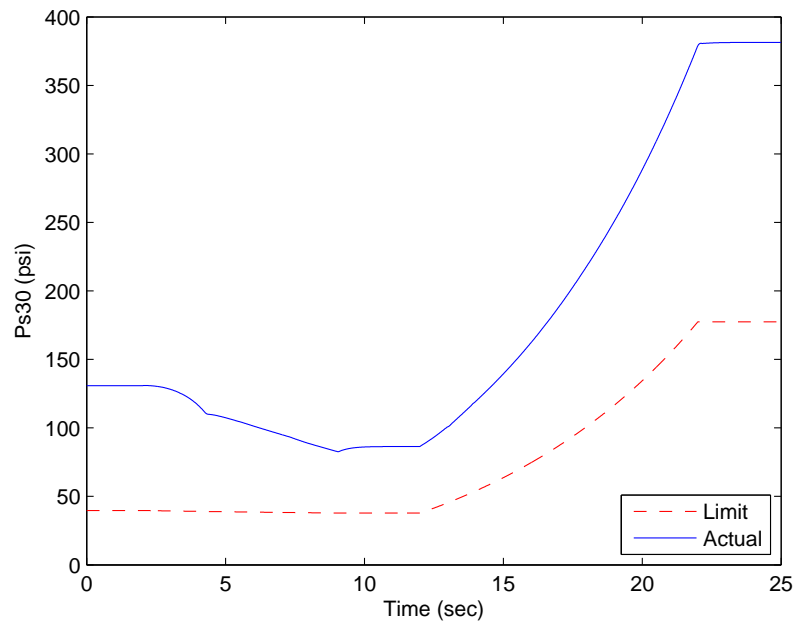Figure 5.28: Core Speed (N_c) vs Time for Long Descent

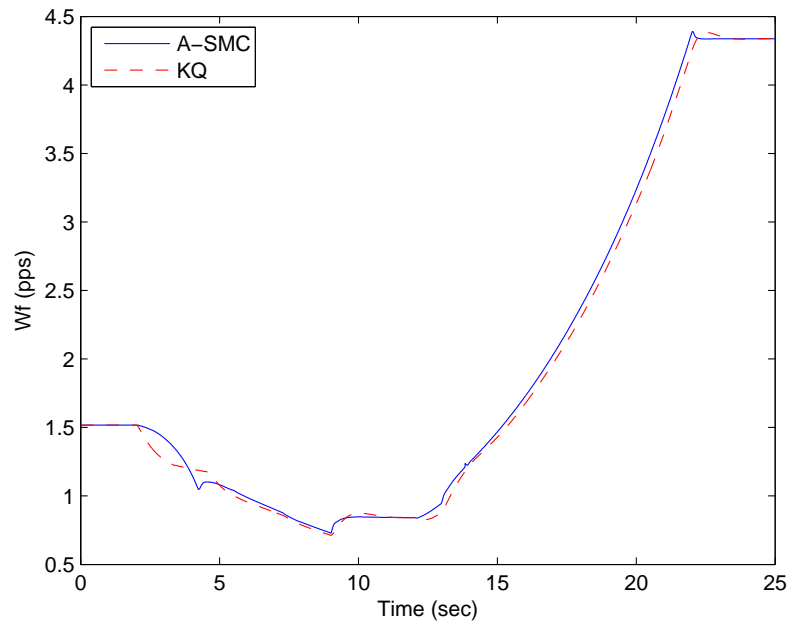Figure 5.29: Burner Static Pressure ($Ps30$) vs Time for Long Descent

64

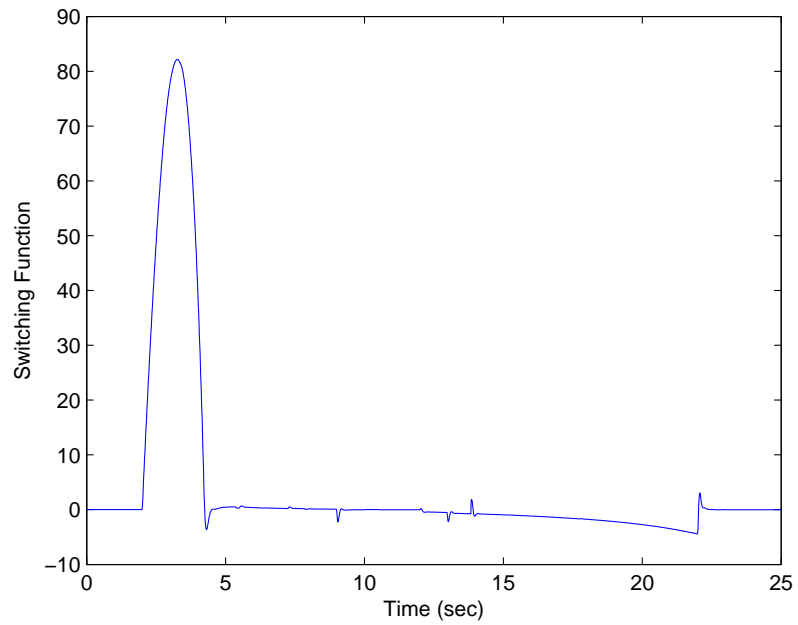Figure 5.30: Fuel Flow (W_f) vs Time for Long Descent

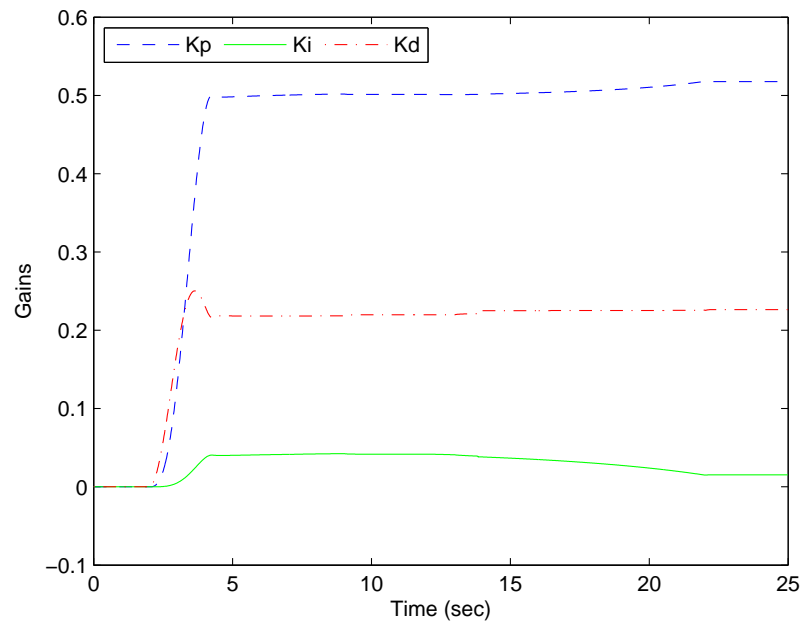Figure 5.31: Fan Speed σ vs Time for Long Descent

65

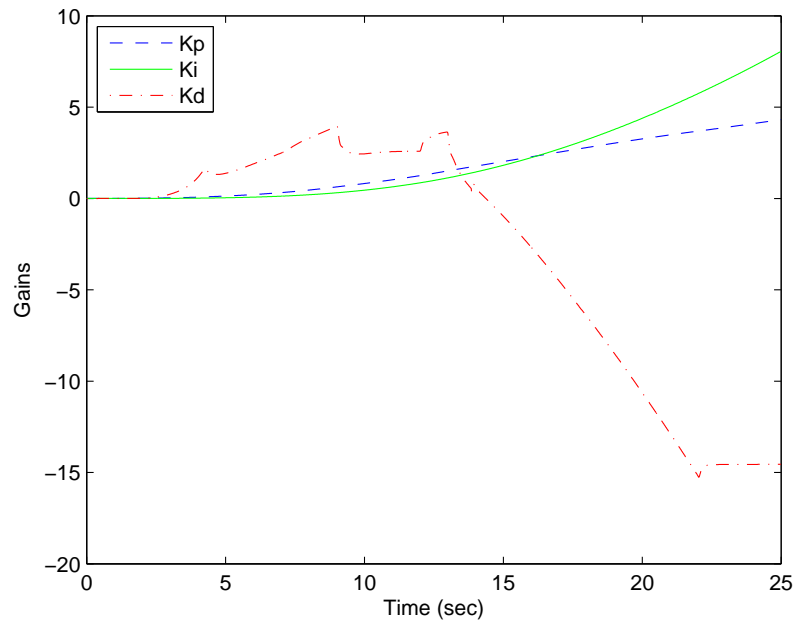Figure 5.32: Fan Speed Adaptive Gains vs Time for Long Descent

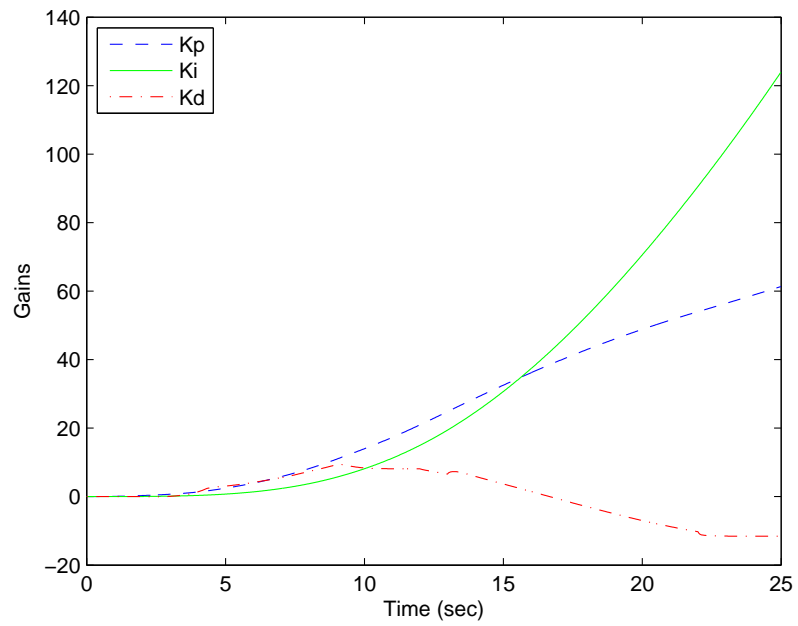Figure 5.33: HPT Exit Temp Adaptive Gains vs Time for Long Descent

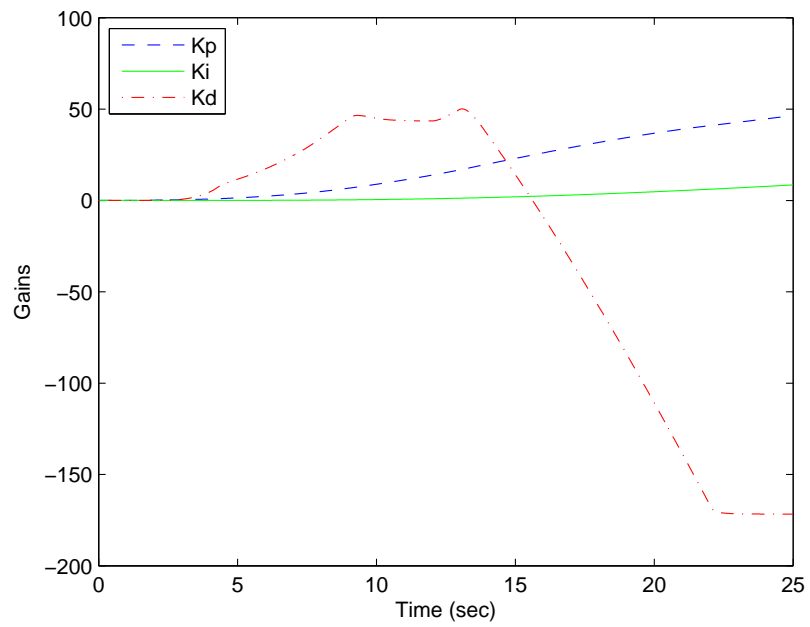Figure 5.34: Engine Pressure Ratio Adaptive Gains vs Time for Long Descent

Figure 5.35: Core Speed Adaptive Gains vs Time for Long Descent
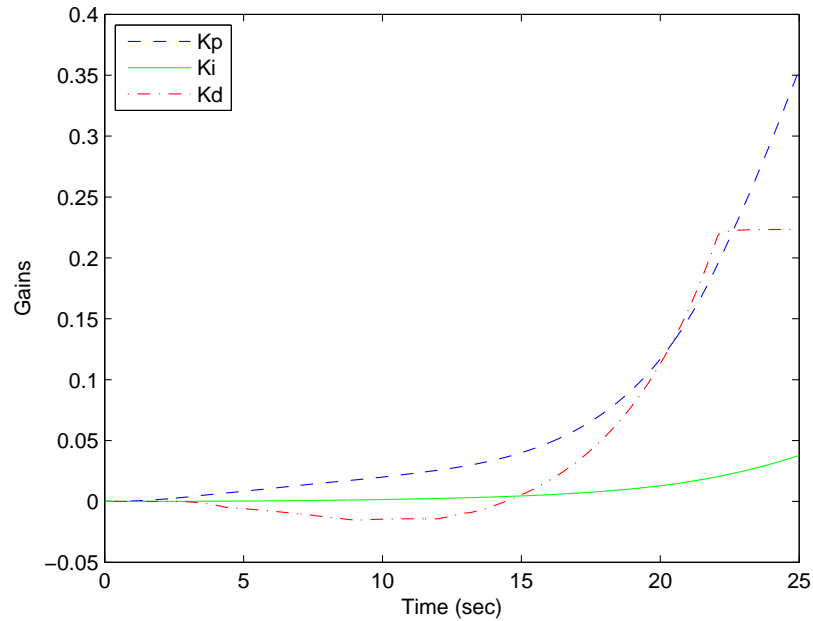
67

Figure 5.36: Burner Static Pressure Adaptive Gains vs Time for Long Descent

5.3.3 Stair Steps Up

The final simulation is of stair steps up where the throttle inputs multiple step inputs successively. The user inputs for C-MAPSS are shown in Figure 5.37.

- Altitude (feet): 25,000 (constant)

- Mach Number: 0.62 (constant)

- Sea Level Temperature: $59\,^\circ F$ (constant)

- TRA: 60° ($t = 0 : 2$ sec), 61° ($t = 2 : 7$ sec), 62° ($t = 7 : 12$ sec), 63° ($t = 12 : 17$ sec), 64° ($t = 17 : 22$ sec), 65° ($t = 22 : 25$ sec)

The results of the simulation are shown in Figures 5.38 through 5.49. Figure 5.38 shows the fan speed response of the A-SMC controller. The adaptability of the A-SMC controller is apparent in this simulation. As the system progresses, the controller more quickly adapts to each step change. The limit regulators are shown in Figures
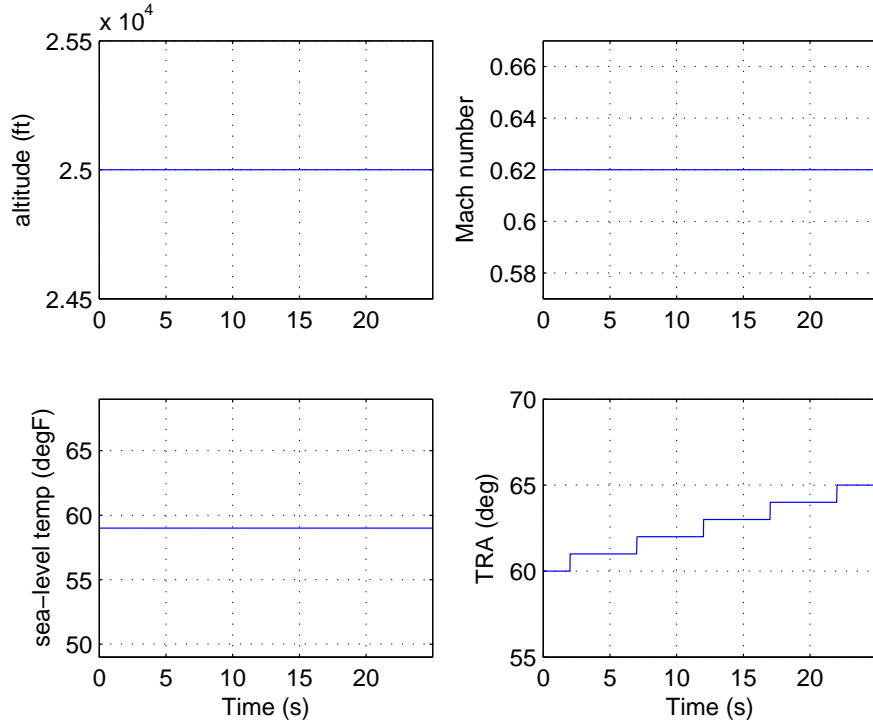
Figure 5.37: User Inputs for Stair Steps Up

5.39 through 5.42. It is shown that the limits are not exceeded because the engine does not require maximum power. A comparison of the fuel flow rate of the A-SMC controller and of the C-MAPSS controller (KQ) is shown in Figure 5.43. The fuel flow rate of the A-SMC is initially slower than that of the KQ controller. However, as it adapts, the A-SMC is able to provide a higher fuel flow rate. Figure 5.44 shows the switching function goes to zero when the system has settled. Finally, the adaptive gains for each A-SMC are given in Figures 5.45 through 5.49. The same results are found here as in the previous simulations. All of the fan speed gains are able to adapt. The K_p and K_i gains for the limit regulators increase and the K_d gains level off.
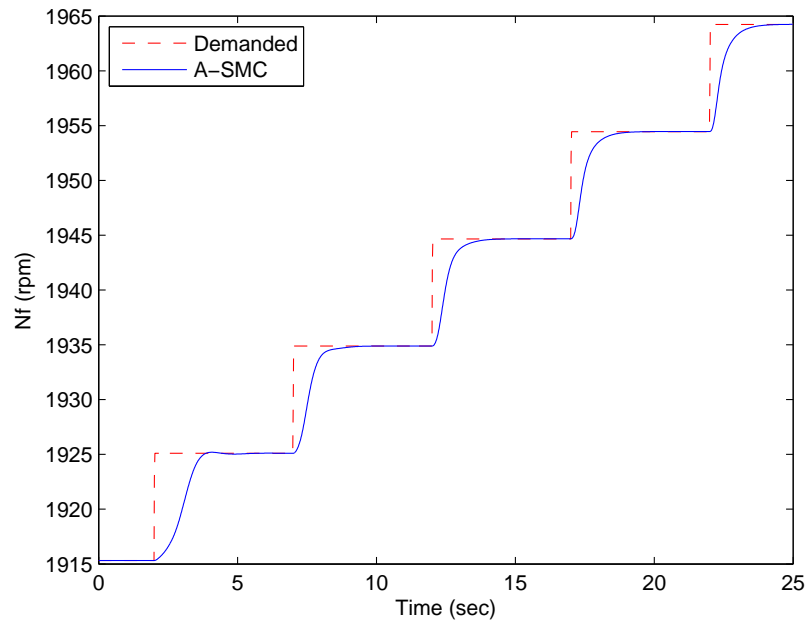
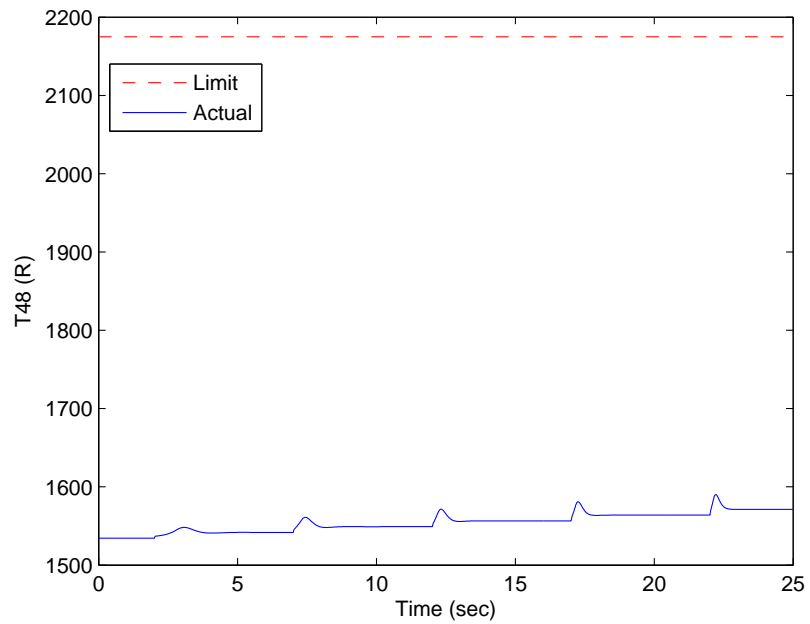Figure 5.38: Fan Speed (N_f) vs Time for Stair Steps Up

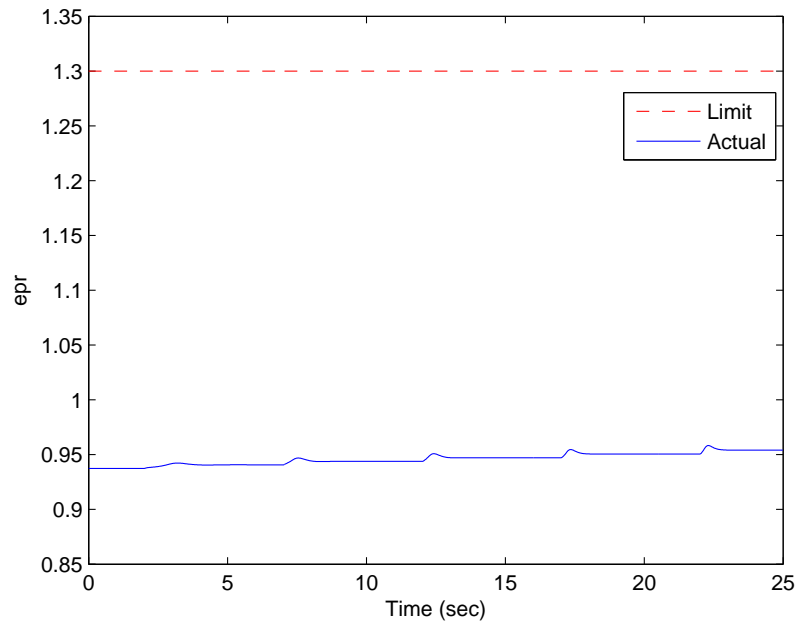Figure 5.39: HPT Exit Temp ($T48$) vs Time for Stair Steps Up

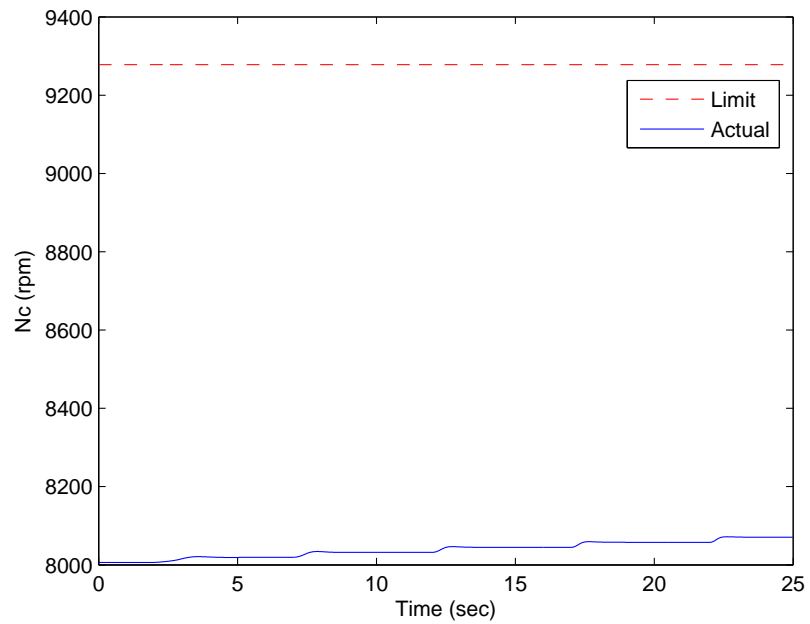Figure 5.40: Engine Pressure Ratio (epr) vs Time for Stair Steps Up

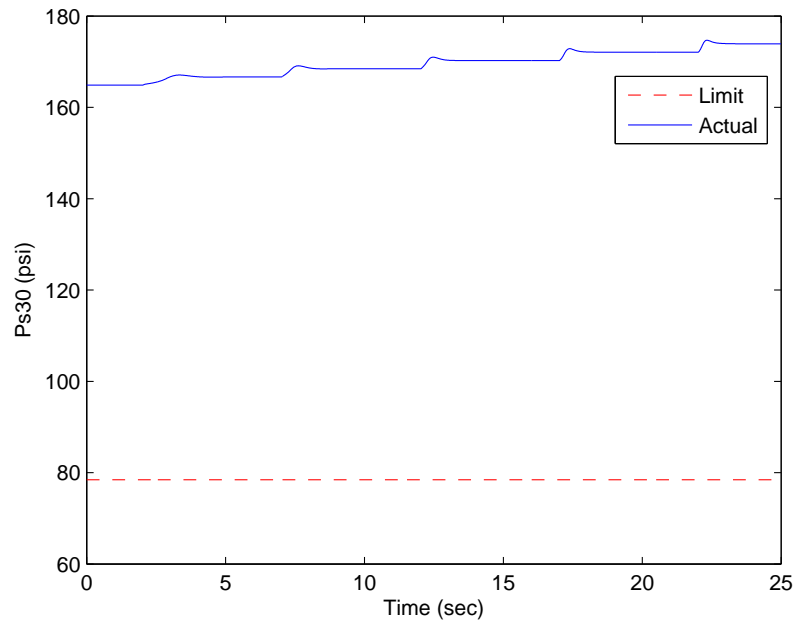Figure 5.41: Core Speed (N_c) vs Time for Stair Steps Up

71

Figure 5.42: Burner Static Pressure ($Ps30$) vs Time for Stair Steps Up
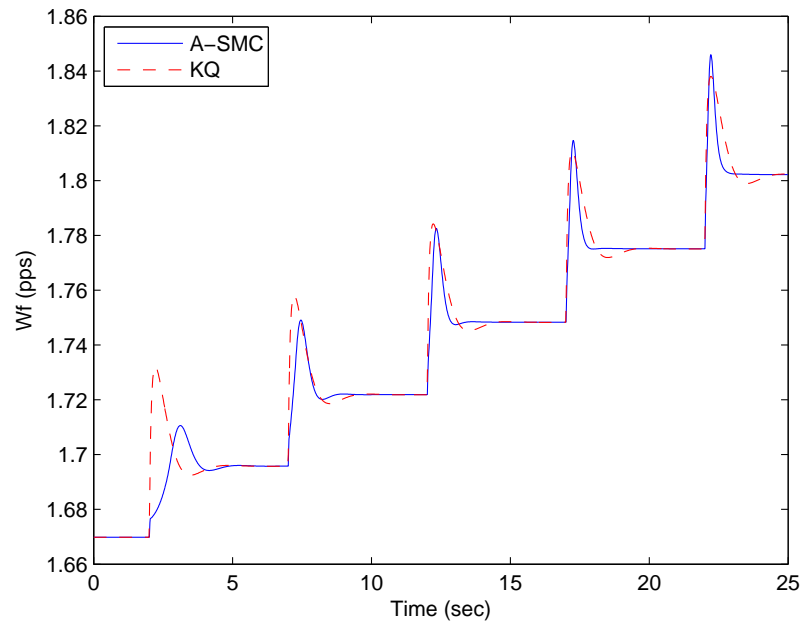
Figure 5.43: Fuel Flow (W_f) vs Time for Stair Steps Up

72

Figure 5.44: Fan Speed σ vs Time for Stair Steps Up

Figure 5.45: Fan Speed Adaptive Gains vs Time for Stair Steps Up

73

Figure 5.46: HPT Exit Temp Adaptive Gains vs Time for Stair Steps Up

Figure 5.47: Engine Pressure Ratio Adaptive Gains vs Time for Stair Steps Up

74

Figure 5.48: Core Speed Adaptive Gains vs Time for Stair Steps Up
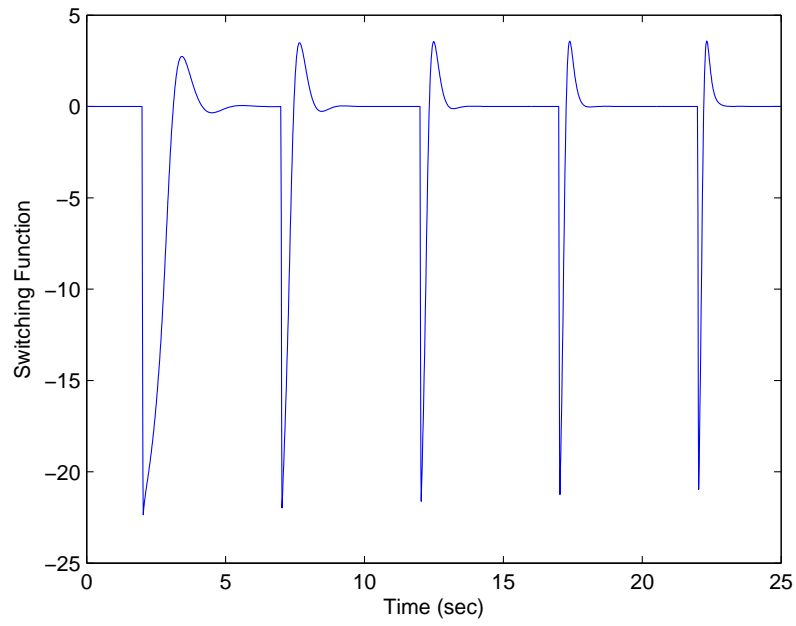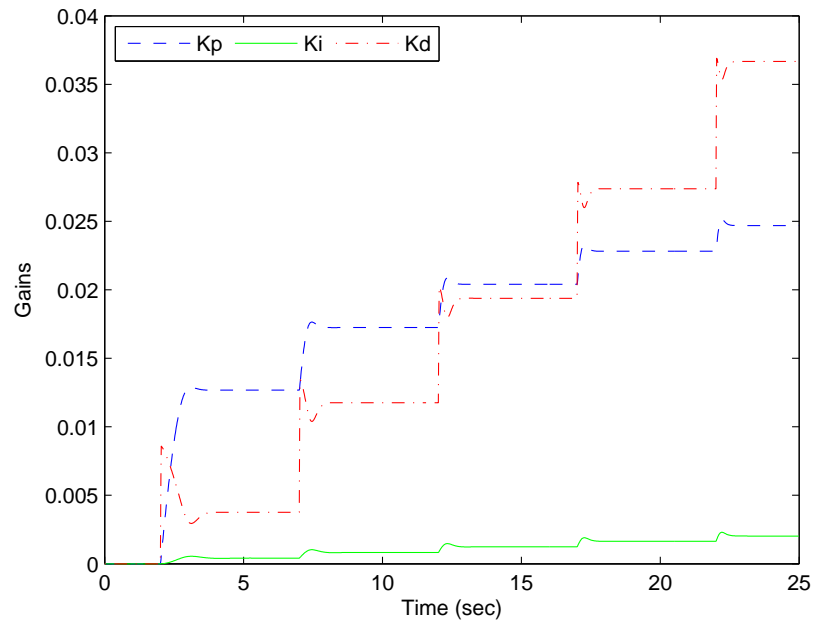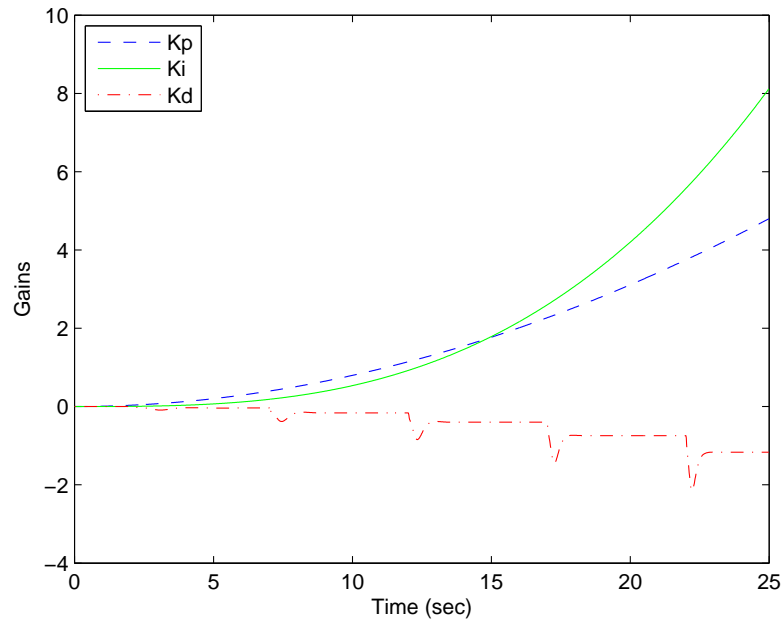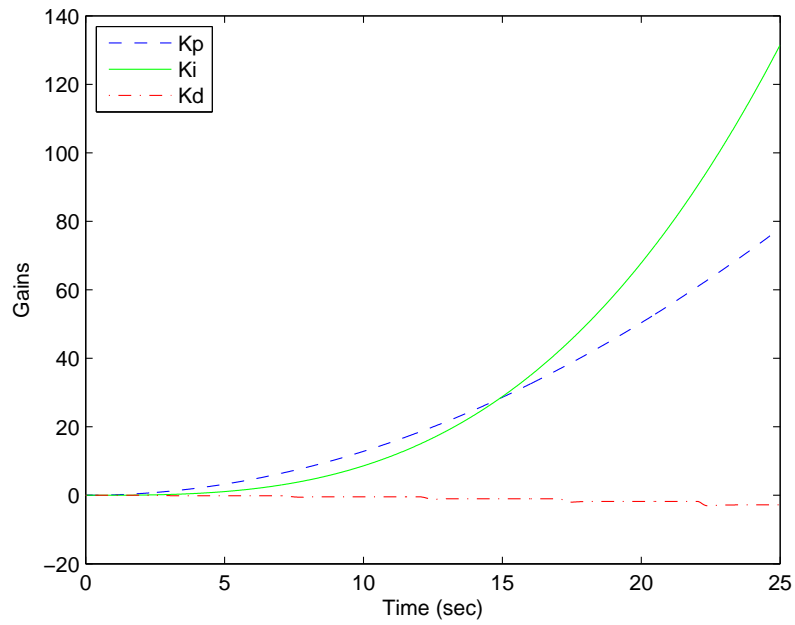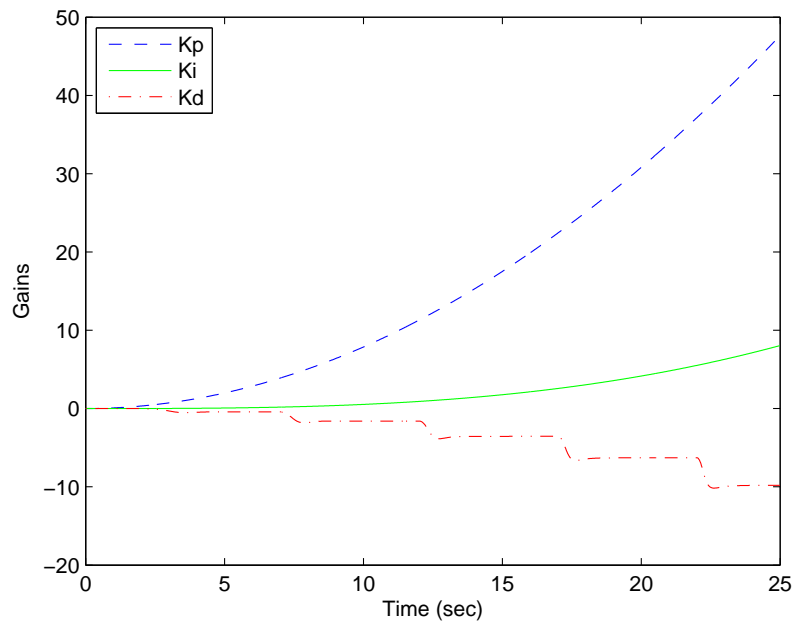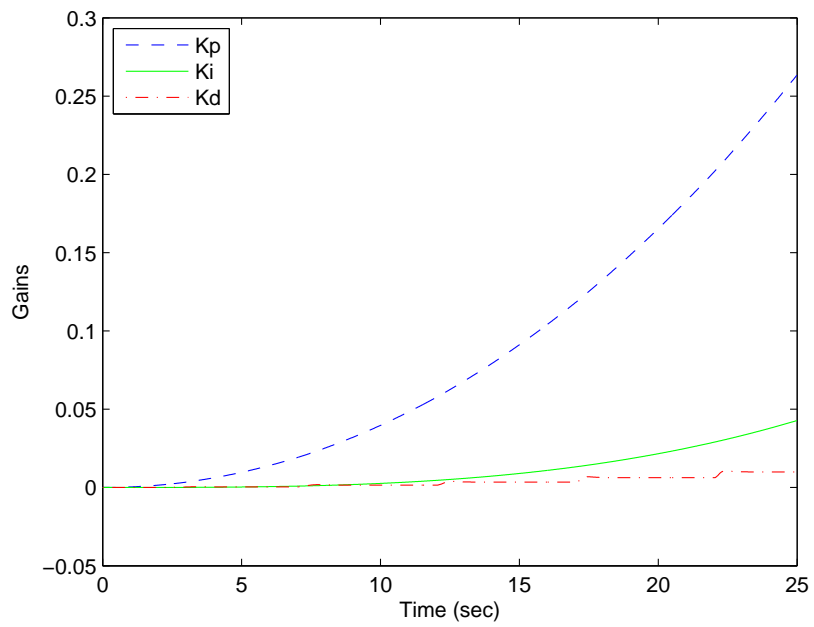

Figure 5.49: Burner Static Pressure Adaptive Gains vs Time for Stair Steps Up

75

CHAPTER VI

CONCLUSIONS AND FUTURE WORK

6.1 Conclusions

The purpose of this thesis was to investigate the feasibility of an adaptive PID sliding mode control on an aircraft engine. The control methodology was developed and applied to a simulated turbofan engine using C-MAPSS. The simulations show the adaptability and robustness of the overall controller. The engine performance was not drastically improved but the A-SMC would eliminate the need for developing the lookup tables used in the gain schedule method.

The simplicity of the PID portion of the controller combined with the robustness of the SMC make this controller a suitable choice for designing an aircraft engine controller. The PID gains are able to adapt for short flight simulations. However, when the engine is operating away from the limits the proportional and integral gains continue to increase. In normal flight scenarios that last for hours, these gains may increase to a level that is too high to adapt when a limit is reached later in flight. Although the robust nature of SMC aids in the reaction time of the limit regulators, it may still be too long. The fan speed controller has already adapted to the flight condition change and is the controller that is selected in the min-max scheme. Since the saturation function is used to deal with the chattering phenomenon the trajectory

is no longer forced to stay on the sliding surface. This leads to a steady state error. By the time that the limit regulators have reacted, the fan speed controller is already within its boundary layer.

6.2   Future Work

The concept of an adaptive sliding mode controller is a good candidate to replace the current gain scheduling scheme that is used for aircraft engines. There are more areas that can be studied using this work as a basis. In this thesis, the boundary layer technique was selected to deal with chattering. A relatively large boundary layer was used making it difficult to switch to another A-SMC in the min-max scheme. There are other methods that can be used to eliminate this undesirable characteristic, such as an observer-based sliding mode control. There are also more areas of aircraft engine control design that were not presented here. The study of engine deterioration still needs to be investigated with the A-SMC. This design method can also be used in a newer, more complete simulation environment, such as C-MAPSS v2.0 or C-MAPSS40k.

The idea of using a sliding mode control scheme for aircraft engine control provides a broad range of areas to study. In this thesis an adaptive SMC was used, however, there are many more facets of SMC that can be investigated for use in this area.

BIBLIOGRAPHY

[1] Wei-Der Chang and Jun-Juh Yan. Adaptive robust PID controller design based on a sliding mode for uncertain chaotic systems. *Chaos Solitons and Fractals*, 26:167–175, 2005.

[2] File:Brayton cycle.svg. `http://en.wikipedia.org/wiki/File:Brayton_cycle.svg`, Accessed November 2011.

[3] Jonathan A. DeCastro, Jonathan S. Litt, and Dean K. Frederick. A modular aero-propulsion system simulation of a large commercial aircraft engine. *National Aeronautics and Space Administration*, 2008.

[4] Richard C. Dorf and Robert H. Bishop. *Modern Control Systems*. Prentice Hall, 2008.

[5] Christopher Edwards and Sarah K. Sprugeon. *Sliding Mode Control: Theory and Applications*. Taylor and Francis, 1998.

[6] Ahmed F. El-Sayed. *Aircraft Propulsion and Gas Turbine Engines*. CRC Press, 2008.

[7] File:Jet engine.svg. `http://en.wikipedia.org/wiki/File:Jet_engine.svg`, Accessed November 2011.

[8] Dean K. Frederick, Jonathan A. DeCastro, and Jonathan S. Litt. User's guide for the commercial modular aero-propulsion system simulation (C-MAPSS). *National Aeronautics and Space Administration*, October 2007.

[9] John Y. Hung, Weibing Gao, and James C. Hung. Variable structure control: A survey. *IEEE Transactions on Industrial Electronics*, 40(1):2–22, 1993.

[10] H. Austin Spang III and Harold Brown. Control of jet engines. *Control Engineering Practice*, 7(9):1043–1059, 1999.

[11] The United States Naval Institute. *Energy Analysis of Naval Machinery.* 1940.

[12] Petros A. Ioannou and Jing Sun. *Robust Adaptive Control.* Prentice Hall, 1995.

[13] T.C. Kuo, Y.J. Huang, C.Y. Chen, and C.H. Chang. Adaptive sliding mode control with PID tuning for uncertain systems. *Engineering Letters*, 16(3), 2008.

[14] Ryan D. May, Jeffrey Csank, Thomas M. Lavelle, Jonathan S. Litt, and Ten-Heui Guo. A high-fidelity simulation of a generic commercial aircraft engine and controller. *National Aeronautics and Space Administration*, 2010.

[15] Khary I. Parker and Ten-Heui Guo. Development of a turbofan engine simulation in a graphical simulation environment. *National Aeronautics and Space Adminstration*, 2003.

[16] Vadim Utkin and Hoon Lee. Chattering problem in sliding mode control systems. *Proccedings of the 2006 International Workshop on Variable Structure Sytems*, pages 346–350, 2006.

[17] V.I. Utkin. Application oriented trends in sliding mode control theory. *International Conference on Industrial Electronics, Control, and Instrumentation, 1993*, 3:1937–1942, 1993.

[18] Link C. Jaw with Jack D. Mattingly. *Aircraft Engine Controls: Design, System Analysis, and Health Monitoring.* American Institute of Aeronautics and Astronautics, 2009.

[19] K. David Young, Vadim I. Utkin, and Umut Ozguner. A control engineer's guide to sliding mode control. *IEEE Transactions on Control Systems Technology*, 7(3):328–342, 1999.

APPENDICES

APPENDIX A

C-MAPSS FLIGHT CONDITION

- Altitude: 0 ft

- Mach Number: 0

- Temperature Sea Level: $59°F$

- TRA: $100°$

- Fuel Flow: 6.835 pps

- Fan Speed: 2388 rpm

- Core Speed: 9051 rpm

- epr: 1.300

- HPT Outlet Temp: $2072°R$

- Net Thrust: 86,336 lbf

APPENDIX B

MATLAB FILES

Variables for A-SMC in C-MAPSS

```
%variables for Fan Speed Controller

gamma_Nf = 30;

wn_Nf = 0.04;

K0_Nf = wn_Nf^2;

K1_Nf = 2*gamma_Nf*wn_Nf;

K2_Nf = 1;

eta1_Nf = 1e-4;

eta2_Nf = 1e-5;

eta3_Nf = 1e-4;

g_Nf = 0;

alpha_Nf = 0;

del_Nf = 10;


A1 = [0 1; 17.4743 8.5637];

a2_Nf=-A1(2,1);

a1_Nf=-A1(2,2);

b_Nf=2032;%ignore zero for design, not for simulation
```

```matlab
%variables for T48 Limit Regulator

gamma_T48 = 1;

wn_T48 = 2;

K0_T48 = wn_T48^2;

K1_T48 = 2*gamma_T48*wn_T48;

K2_T48 = 1;

eta1_T48 = 1e-8;

eta2_T48 = 1e-9;

eta3_T48 = 1e-6;

g_T48 = 0;

alpha_T48 = 0;

del_T48 = 10;


A2 = [0 1; -17.4743 -8.5637];

a2_T48=-A2(2,1);

a1_T48=-A2(2,2);

b_T48=1595;%ignore zero for design, not for simulation



%variables for Ps30 Limit Regulator

gamma_Ps30 = 2.075;

wn_Ps30 = 1;

K0_Ps30 = wn_Ps30^2;

K1_Ps30 = 2*gamma_Ps30*wn_Ps30;

K2_Ps30 = 1;

eta1_Ps30 = 1e-7;

eta2_Ps30 = 1e-9;

eta3_Ps30 = 1e-6;
```

```matlab
g_Ps30 = 0;

alpha_Ps30 = 0;

del_Ps30 = 10;


A2 = [0 1; -17.4743 -8.5637];

a2_Ps30=-A2(2,1);

a1_Ps30=-A2(2,2);

b_Ps30=962;%ignore zero for design, not for simulation



%variables for epr Limit Regulator

gamma_epr = 0.707;

wn_epr = 1.414;

K0_epr = wn_epr^2;

K1_epr = 2*gamma_epr*wn_epr;

K2_epr = 1;

eta1_epr = 1;

eta2_epr = 0.1;

eta3_epr = 10;

g_epr = 0;

alpha_epr = 0;

del_epr = 0.1;


A2 = [0 1; -17.4743 -8.5637];

a2_epr=-A2(2,1);

a1_epr=-A2(2,2);

b_epr=1.026;%ignore zero for design, not for simulation
```

```
%variables for Core Speed Regulator

gamma_Nc = 1.69;

wn_Nc = 1;

K0_Nc = wn_Nc^2;

K1_Nc = 2*gamma_Nc*wn_Nc;

K2_Nc = 1;

eta1_Nc = 1e-7;

eta2_Nc = 1e-9;

eta3_Nc = 1e-5;

g_Nc = 0;

alpha_Nc = 0;

del_Nc = 10;


A1 = [0 1; -17.4743 -8.5637];

a2_Nc=-A1(2,1);

a1_Nc=-A1(2,2);

b_Nc=2628;%ignore zero for design, not for simulation
```